2015

From soilscapes to landscapes: A landscape-oriented approach to simulate soil organic carbon dynamics in intensively managed landscapes

A. N. Papanicolaou
University of Tennessee, tpapanic@utk.edu

Kenneth M. Wacha
University of Iowa

Benjamin K. Abban
University of Tennessee

Christopher G. Wilson
University of Tennessee

Jerry L. Hatfield
USDA-ARS, jerry.hatfield@ars.usda.gov

See next page for additional authors

AGU PUBLICATIONS

JGR

Journal of Geophysical Research: Biogeosciences

RESEARCH ARTICLE
10.1002/2015JG003078

Key Points:
- Conservation tillage and enhanced crop yields produce gains in soil organic carbon
- Enrichment ratio and bulk density vary spatially and temporally in intensively managed fields
- Management practices and hillslope location affect soil organic carbon dynamics

Correspondence to:
A. N. (T.) Papanicolaou,
tpapanic@utk.edu

Citation:
Papanicolaou, A. N. (T.), K. M. Wacha, B. K. Abban, C. G. Wilson, J. L. Hatfield, C. O. Stanier, and T. R. Filley (2015), From soilscapes to landscapes: A landscape-oriented approach to simulate soil organic carbon dynamics in intensively managed landscapes, *J. Geophys. Res. Biogeosci.*, *120*, 2375–2401, doi:10.1002/2015JG003078.

Received 4 JUN 2015
Accepted 7 OCT 2015
Accepted article online 11 OCT 2015
Published online 25 NOV 2015

From soilscapes to landscapes: A landscape-oriented approach to simulate soil organic carbon dynamics in intensively managed landscapes

A. N. (Thanos) Papanicolaou[1], Kenneth M. Wacha[2], Benjamin K. Abban[1], Christopher G. Wilson[1], Jerry L. Hatfield[3], Charles O. Stanier[4], and Timothy R. Filley[5]

[1]Hydraulics and Sedimentation Laboratory, Department of Civil and Environmental Engineering, University of Tennessee, Knoxville, Knoxville, Tennessee, USA, [2]IIHR, Hydroscience and Engineering, Department of Civil and Environmental Engineering, University of Iowa, Iowa City, Iowa, USA, [3]USDA-ARS National Laboratory for Agriculture and the Environment, Ames, Iowa, USA, [4]IIHR, Hydroscience and Engineering, Department of Chemical and Biochemical Engineering, University of Iowa, Iowa City, Iowa, USA, [5]Department of Earth, Atmospheric and Planetary Sciences, Purdue University, West Lafayette, Indiana, USA

Abstract Most available biogeochemical models focus within a soil profile and cannot adequately resolve contributions of the lighter size fractions of organic rich soils for enrichment ratio (ER) estimates, thereby causing unintended errors in soil organic carbon (SOC) storage predictions. These models set ER as constant, usually equal to unity. The goal of this study is to provide spatiotemporal predictions of SOC stocks at the hillslope scale that account for the selective entrainment and deposition of lighter size fractions. It is hypothesized herein that ER values may vary depending on hillslope location, Land Use/Land Cover (LULC) conditions, and magnitude of the hydrologic event. An ER module interlinked with two established models, CENTURY and Watershed Erosion Prediction Project, is developed that considers the effects of changing runoff coefficients, bare soil coverage, tillage depth, fertilization, and soil roughness on SOC redistribution and storage. In this study, a representative hillslope is partitioned into two control volumes (CVs): a net erosional upslope zone and a net depositional downslope zone. We first estimate ER values for both CVs I and II for different hydrologic and LULC conditions. Second, using the improved ER estimates for the two CVs, we evaluate the effects that management practices have on SOC redistribution during different crop rotations. Overall, LULC promoting less runoff generally yielded higher ER values, which ranged between 0.97 and 3.25. Eroded soils in the upland CV were up to 4% more enriched in SOC than eroded soils in the downslope CV due to larger interrill contributions, which were found to be of equal importance to rill contributions. The chronosequence in SOC storage for the erosional zone revealed that conservation tillage and enhanced crop yields begun in the 1980s reversed the downward trend in SOC losses, causing nearly 26% of the lost SOC to be regained.

1. Introduction

Soil organic carbon (SOC) is an important constituent of the Earth's fabric derived from the breakdown of aboveground plant residue, plant rhizomes, and root exudates. In intensively managed landscapes (IMLs), determining the SOC storage potential is of high importance for sustaining soil quality and crop productivity [e.g., *Andrews et al.*, 2002; *Sperow et al.*, 2003; *Cambardella et al.*, 2004; *Lal*, 2011], as well as for mitigating rising Carbon Dioxide (CO_2) levels in the atmosphere [e.g., *Houghton*, 2008; *Kuhn et al.*, 2009; *Hatfield and Parkin*, 2012].

Several studies conducted over the last quarter of the century have emphasized the understanding of key biogeochemical processes affecting "above" and "below" ground carbon allocation, as well as other aspects of carbon dynamics and storage [e.g., *Smith and Paul*, 1990; *Paustian et al.*, 1992, 2006; *Gregorich et al.*, 1998; *Richter et al.*, 1999; *Metting et al.*, 1999; *Lal*, 2004; *Polyakov and Lal*, 2004; *Jacinthe et al.*, 2009; *Kuhn et al.*, 2009; *Du and Walling*, 2011; *Li et al.*, 2012; *Navas et al.*, 2012; *Zhang et al.*, 2013]. Despite considerable gains in knowledge about SOC processes, most of these studies have been geospatially limited to the soil profile, thereby failing to account for the effects of landscape heterogeneity on SOC redistribution and storage [e.g., *Tornquist et al.*, 2009]. In addition, the majority of the studies has been performed in punctually disturbed ecosystems, such as grasslands and forests, rather than constantly disturbed IMLs [e.g., *Li et al.*, 1997; *Yoo et al.*, 2005; *Parton et al.*, 2007].

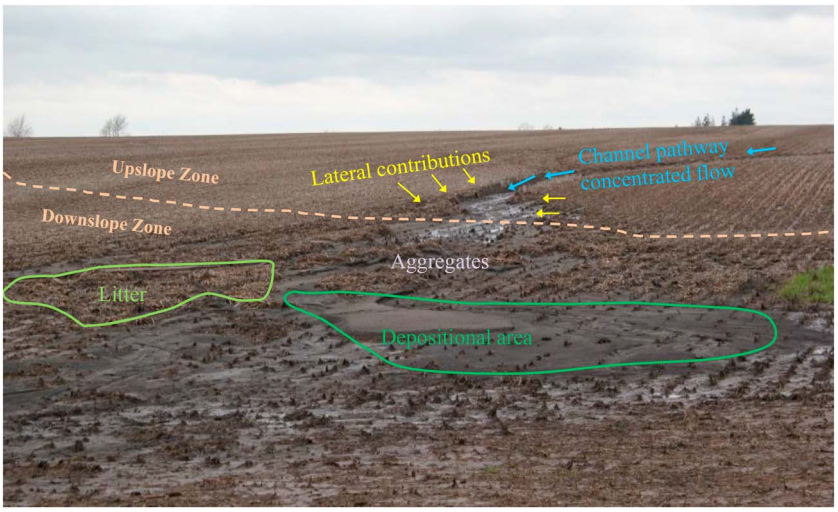

Figure 1. Soil and SOC redistribution. In an agricultural farm field, the collective effects of rain splash-/runoff- and tillage-induced erosion/deposition redistribute finer soil particles and SOC heterogeneously along the hillslope.

Only a handful of models have the capacity to incorporate the effects of rainsplash/runoff and tillage erosion, defined herein as "collective erosion," and deposition on SOC predictions at watershed scales [*Van Oost et al*., 2000, 2005]. Rainsplash triggers redistribution of the finer fractions of soil through sheet erosion with lateral inputs to rills (Figure 1). Rills, in turn, erode on their own due to concentrated flows and convey the total eroded material downslope from erosion-dominated areas to deposition-dominated areas (Figure 1). Tillage has several effects on SOC redistribution and storage potential through a series of mechanistic processes [*Moore and Burch*, 1986; *Van Oost et al*., 2000; *Billings et al*., 2010; *Lal*, 2011]. These include the incorporation of residue within the soil profile (Figure 1) and fracturing of soil aggregates which exposes lighter size fractions of carbon-enriched material to selective entrainment by flow [*Kuhn et al*., 2009; *Papanicolaou et al*., 2009; *Van Oost et al*., 2009]. Selective entrainment of the lighter size fractions affects the enrichment ratio (ER), which is a unique measure of change in available SOC through the enrichment or depletion of the finer size fraction of organic rich soils [*Palis et al*., 1990; *Wang et al*., 2013].

Changes in Land Use/Land Cover (LULC) and associated management practices in agricultural IMLs can lead to a higher degree of spatial heterogeneity and temporal variability in SOC redistribution during crop rotations uncommon in other systems [*Parkin*, 1993; *Abaci and Papanicolaou*, 2009; *Dlugoß et al*., 2010; *Kravchenko and Robertson*, 2011; *Du and Walling*, 2011; *Stavi and Lal*, 2011; *Navas et al*., 2012]. These different practices lead to changes in the percentage of bare soil, tillage depth, fertilization, and soil roughness. The degree that these changes influence SOC redistribution and storage may vary depending on the hillslope location and the magnitude of the hydrologic event. In fact, SOC changes may be significantly different in erosion-dominated (i.e., upslope) areas of a hillslope versus deposition-dominated (i.e., downslope) areas, with significant effects on net gains or losses in the SOC stored in these zones [*Van Oost et al*., 2006; *Wang et al*., 2015]. It is, therefore, not surprising that most of the available biogeochemical models, being soil profile models or "point models in space," tend to overestimate or underestimate SOC storage predictions in IMLs as they do not account for outputs or inputs of mobilized SOC [e.g., *Parton et al*., 1987; *Paustian et al*., 1992; *Harden et al*., 1999; *Manies et al*., 2001; *Mangan et al*., 2004; *Jarecki et al*., 2008; *Tornquist et al*., 2009; *Wilson et al*., 2009; *Van Oost et al*., 2006; *Bortolon et al*., 2011; *van Groenigen et al*., 2011; *Vaccari et al*., 2012].

Some studies have linked existing biogeochemical models (e.g., Rothamsted Carbon (ROTH-C), DNDC (DeNitrification-DeComposition), and CENTURY) with lumped erosion models, such as those based on the Universal Soil Loss Equation or its modifications [e.g., *Monreal et al*., 1997; *Manies et al*., 2001; *Zhang et al*., 2014], to account for losses of SOC along the downslope. These erosion models tend to provide long-term (100 year time window) estimates of eroded SOC fluxes, but are neither meant to capture the seasonal variability in SOC distribution [*Harden et al*., 1999; *Li et al*., 1997; *Blaschke and Hay*, 2001] nor account for SOC deposition [*Gregorich et al*., 1998; *Van Oost et al*., 2006].

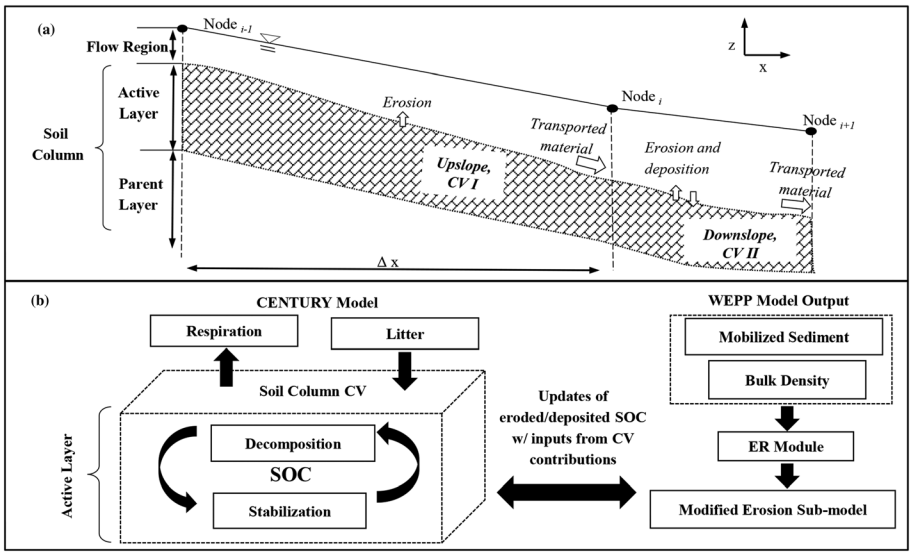

Figure 2. Linked WEPP-CENTURY modeling framework. A hillslope is segmented into control volume (CV) sections composed of a flow region, soil active layer, and parent layer. (a) The WEPP model and ER module are used to simulate the mobilization, transport, and deposition of soil size fractions and SOC along the hillslope. (b) The integrative modeling framework allows the CV active layer to be updated via redistribution (from Figure 2a) as well as physical mechanisms (processes) of decomposition, stabilization, and incorporation.

Recently, significant modeling efforts have accounted for the dynamics of collective erosion and the role of deposition on SOC redistribution and storage [e.g., *Billings et al*., 2010; *Dlugoß et al*., 2010, 2012]. However, these models do not adequately incorporate the effects of selective entrainment and deposition of the finer size fraction of organic rich soils by the flow [*Van Oost et al*., 2005; *Dlugoß et al*., 2010, 2012]. The ER is currently assumed to be equal to unity [*Teixeira and Misra*, 1997] or to obtain a constant value greater than unity. On the contrary, it is anticipated that the range of ER values may vary depending on hillslope location and the magnitude of the hydrologic event leading to an overestimation of the SOC displaced [*Kuhn et al*., 2009; *Thompson et al*., 2010; *Hu et al*., 2013].

The goal of this study is to provide spatiotemporal predictions of SOC stocks at the hillslope scale by accounting for the role of selective entrainment and deposition on SOC redistribution under different hydrologic and LULC conditions. SOC predictions are made following a similar discretization approach suggested by *Berhe et al*. [2012] where the hillslope is partitioned into two control volumes (CVs): an upslope zone and downslope zone illustrated in Figure 2a. An ER module is developed to account for selective entrainment and deposition in both zones. The backbone of the proposed modeling framework is based on the recognition that (1) interrill splash erosion is of equal importance to rill erosion for soil dislodgement and therefore should not be ignored in estimating ER for both the upslope (CV I) and downslope (CV II) zones [*Hu et al*., 2013] and (2) ER estimations for CV II are strongly affected by material contributions from CV I which in turn affect the potential for material mobilization or settling in CV II under different hydrologic and LULC conditions.

The proposed landscape-oriented approach is demonstrated at the hillslope scale (0.01 km^2) in a case study site of the U.S. Midwest, namely, Clear Creek, IA. The Clear Creek watershed is an ideal location for resolving SOC fluxes due to the data availability on soil, hydrologic, and land use properties [*Papanicolaou and Abaci*, 2008; *Abaci and Papanicolaou*, 2009].

We first estimate ER values for both CVs I and II at the hillslope scale for different hydrologic and LULC conditions. Second, using the improved ER estimates for the two CVs, we evaluate the effects that management practices with different crop cover, tillage depths, fertilization, and soil roughness characteristics have on SOC redistribution in CVs I and II. The simulations are supplemented with detailed site historic and current management practices as well as climate data (benchmark dates of the different management practices within the simulation period are detailed in section 3.2). To assess the predictive capabilities of the newly

developed framework, samples collected from representative field locations in Clear Creek for recent years are compared with model predictions.

2. Integrative WEPP-CENTURY Models

We consider the coupling of two established process-based models, namely, the Watershed Erosion Prediction Project, WEPP (version 2012.8) and the biogeochemical soil-column model, CENTURY (version 4.6). Detailed reviews of WEPP and CENTURY are not the focus here as they have already been presented in past publications [*Flanagan et al*., 2007; *Parton et al*., 1987; *Tornquist et al*., 2009]. Instead, the emphasis is placed here on the steps involved in the coupling of the two models and the ER module.

The coupling of WEPP with CENTURY (Figure 2b) occurs here in a "loose" sense. The soil profile within a CV represents the spatial domain of the CENTURY model. It composes a top layer, known as the active layer (usually the top 20 cm in the soil profile [*Papanicolaou et al*., 2010]), and a lower subhorizon layer, known as the parent layer. CENTURY simulates changes of SOC stocks within the soil active layer through inputs from residue incorporation and losses by decomposition [e.g., *Parton et al*., 1987; *Jarecki et al*., 2008; *Tornquist et al*., 2009; *Wilson et al*., 2009; *Vaccari et al*., 2012; *Zhang et al*., 2013]. However, CENTURY alone cannot explicitly simulate the SOC fluxes entering or exiting the soil profile via the action of collective erosion [*Campbell et al*., 1996; *Metting et al*., 1999].

The role of WEPP is to supplement these missing features in CENTURY. WEPP simulations can capture the downslope variability of key soil parameters (e.g., surface roughness, dry bulk density, critical erosional strength, and hydraulic conductivity) and provide textural updates of the active layer [*Foster*, 1982; *Nearing and Nicks*, 1998; *Pieri et al*., 2007], all of which can strongly influence SOC fluxes.

However, WEPP in its present form cannot adequately resolve contributions of rill and interrill areas on ER estimates [*Vázquez et al*., 2005; *Thompson et al*., 2010] and is unable to simulate the ER of material being deposited within a CV as it tracks only the ER of material exiting from a CV [*Flanagan and Nearing*, 2000].

To address these limitations, an ER module is developed, which is interlinked with WEPP and CENTURY. The module considers separate transport capacity formulae for rill and interrill erosion [*Yalin*, 1963; *Abrahams et al*., 2001] aiming to provide improved estimates of selective entrainment and deposition for both rill and interrill erosion processes. The separate capacity formulae for rill and interrill areas allow for a better representation of different soil size fraction redistribution and associated SOC enrichment for each of the two zones. For CV I, enrichment is calculated for net erosion as the ratio of the concentration of the eroded fraction contributed by rill and interrill processes to the total available concentration found in the active layer prior to an event (see equation (13)). Alternatively, enrichment for CV II is calculated for either net erosion or deposition depending on the "direction" of the net flux. Direction is strongly affected by the material contributions from CV I. Positive direction is defined here as net erosion, whereas negative directions as net deposition. In the case of net erosion, the ER in CV II is calculated similarly as in CV I. In the case of net deposition, the ER in CV II is calculated as the ratio of the concentration of the deposited material fraction in CV II to the concentration of the material fraction eroded from CV I derived by rill and interrill processes (see equation (14)).

The daily outputs of updated ER values along with the daily net soil fluxes and size fractions from the ER module and WEPP are aggregated to a monthly time scale and input into CENTURY to determine SOC stocks within a CV. Updates on SOC stocks due to the effects of decay and physicochemical stabilization of SOC are also estimated.

The following subsections describe the assumptions of the proposed landscape-oriented approach, as well as the enhanced erosion process formulation that the new framework offers.

2.1. Modeling Assumptions

The proposed landscape-oriented approach is based on the following assumptions:

1. The distribution of rainfall is uniformly applied to the CVs at the hillslope scale [*Elhakeem and Papanicolaou*, 2009]. Soil properties within each CV are treated as homogeneous but heterogeneous between the two CVs, which are updated during the simulations.
2. The impact of tillage events is to exacerbate the effects of rainfall-runoff erosion on SOC stocks rather than directly displacing soil in the downslope [*Quine et al*., 1999; *Van Oost et al*., 2005].

3. A fixed fraction of the SOC transported in runoff is considered to be mineralized so that the C loss due to mineralization of SOC in the transported soil can be estimated by a simple relation. In our study it is assumed that 20% of the mobilized material is mineralized [*Lal*, 2006; *Yadav and Malanson*, 2009].
4. Soil is mobilized and transported through both interrill and rill processes [*Zhang et al*., 2003; *Wang et al*., 2013], where rainsplash effects dominate the interrill areas [e.g., *Gilley et al*., 1985; *Gabet and Dunne*, 2003] and concentrated overland flow is the main driver for soil particle movement in rills [e.g., *Römkens et al*., 2002; *Rieke-Zapp and Nearing*, 2005].
5. The capacity of a soil particle to bind SOC is proportional to its surface area and the affinity of its surface to hold carbon [*Palis et al*., 1997; *Thevenot et al*., 2010; *Wäldchen et al*., 2012; *Wang et al*., 2013].
6. The soil continuum is composed of both primary particles and aggregates [*Foster et al*., 1985]. The primary particles (i.e., clay, silt, and sand) are each assigned their median diameters. Aggregates are partitioned into small and large aggregates, with specific gravity values of 1.8 and 1.6, respectively. The size distribution and composition of mobilized soil particles is based on the availability of the range of size fractions found within the active layer of the soil column [*Foster et al*., 1985]. Rill and interrill areas are source contributors of different size fractions to the active layer. The eroding zone is treated as supply limited (i.e., no incoming material from upslope sections) [*Yalin*, 1963; *Abrahams et al*., 2001].
7. Surface residue is distributed homogenously across the soil surface of each CV and is incorporated vertically within the soil active layer profile during a tillage event [*Salinas-García et al*., 2002; *Flanagan et al*., 2012].
8. SOC biogeochemical stabilization within the active layer is treated as a continuous process that includes not only supply contributions from decayed labile forms of SOC, such as root exudates and residue leachates, but also the decayed portions of incorporated residue and roots, which are relatively more decay resistant than fresh plant material [*Six et al*., 2002; *Olchin et al*., 2008].

2.2. Enhanced Model Formulation

In the sections below, we provide the basic relationship used to estimate SOC stocks within the active layer followed by the key formulation for estimating daily soil fluxes, enrichment ratios, textural updates of the active layer, and related monthly-aggregated SOC fluxes and changes.

Updates in soil flux inputs/outputs along with updates in textural and soil microclimate conditions affect rates of decomposition, stabilization, and respiration within the soil profile [*Paustian et al*., 2006]. Appendix A provides key formulation for the hydrologic component and Appendix A describes formulation for the decomposition, stabilization, and respiration processes. All formulation is presented below in index notation.

2.2.1. Estimation of SOC Stocks Within the Active Layer

The stock of SOC (g C/m^2) present within the active layer of CV i at time j, $(SOC_{\mathrm{ACT}})_i^j$, is defined as follows:

$$(SOC_{\mathrm{ACT}})_i^j = \left(\rho_{\mathrm{Bulk}_{\mathrm{ACT}}}\left(\frac{M_{\mathrm{Carbon}_{\mathrm{ACT}}}}{M_{\mathrm{Soil}_{\mathrm{ACT}}}}\right)D_{\mathrm{ACT}}\right)_i^j \tag{1}$$

where $\rho_{\mathrm{Bulk}_{\mathrm{ACT}}}$ is the dry soil bulk density of the active layer at time j (g/m^3); $M_{\mathrm{Carbon}_{\mathrm{ACT}}}$ is the mass of carbon in the active layer (g); $M_{\mathrm{Soil}_{\mathrm{ACT}}}$ is the mass of soil within the active layer (g); and D_{ACT} is the active layer depth (m).

Studies in agricultural fields have shown that the dry bulk density values can fluctuate subseasonally or seasonally via management and microclimate perturbations [*Logsdon and Karlen*, 2004; *Osunbitan et al*., 2005; *Burras et al*., 2005]. To reflect these changes, we estimate the dry bulk density within the soil active layer, $\rho_{\mathrm{Bulk}_{\mathrm{ACT}}}$, of CV i at time j, with (assumption 2):

$$\left(\rho_{\mathrm{bulk}_{\mathrm{ACT}}}\right)_i^j = (\rho_{\mathrm{till}})_i^j + (\Delta\rho_{rf} + \Delta\rho_{wt})_i^{j-DTE} \tag{2}$$

where ρ_{till} is the dry bulk density value following a particular tillage event (g/m^3); DTE is the number of days since the last tillage disturbance; $\Delta\rho_{\mathrm{rf}}$ is the increase in density due to rainfall consolidation (g/m^3); and $\Delta\rho_{\mathrm{wt}}$ is the increase in density due to weathering consolidation (g/m^3) that is mostly triggered by heavy equipment [e.g., *Williams et al*., 1984; *Flanagan et al*., 2007].

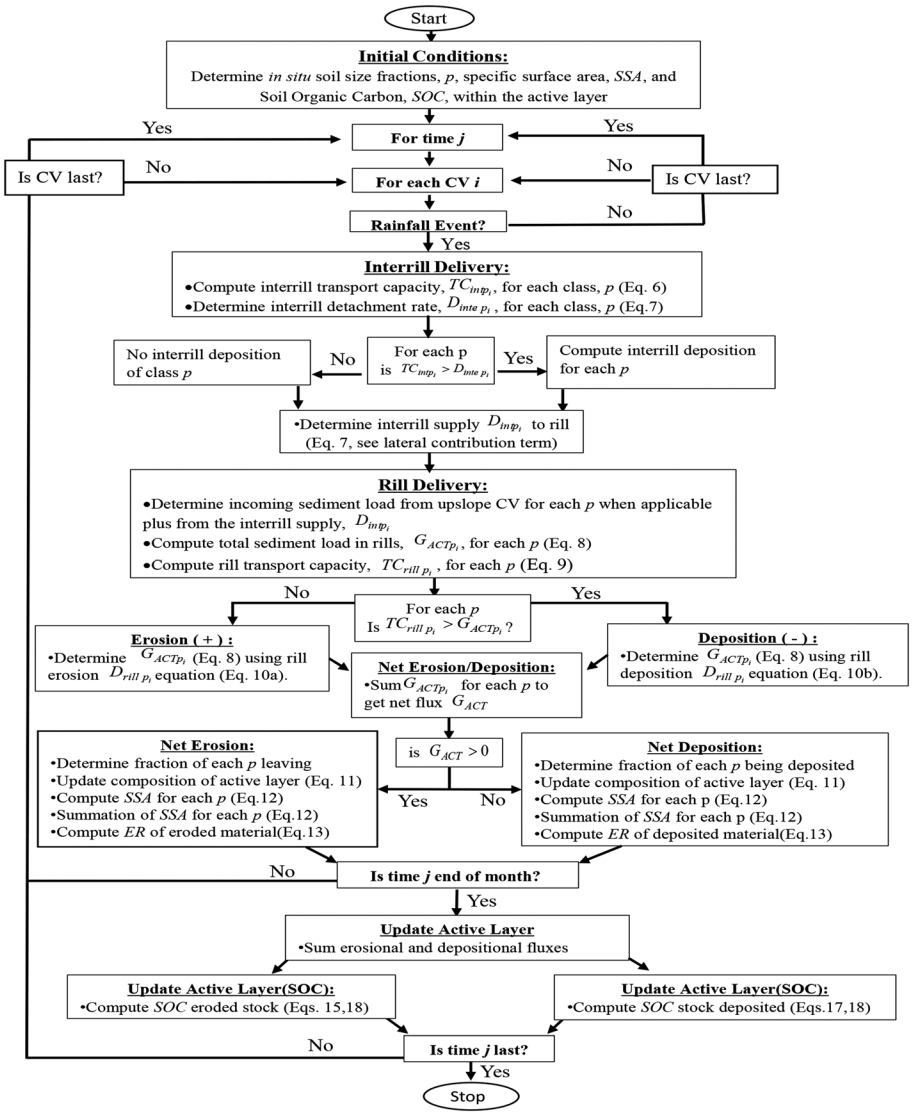

Figure 3. ER module and SOC stock updates. The enrichment ratios and SOC stock updates in the upslope and downslope zones are determined taking into account the mobilization and deposition of the different size fractions in both rill and interrill areas. The ER module considers the flow transport capacity in each area of the CV and updates the composition of the active layer with each event.

2.2.2. Estimation of Net Soil Fluxes and ER—"The ER Module"

The steps involved in estimating the net soil fluxes and ER for daily rainfall-runoff events via WEPP and the ER module are outlined in Figure 3 and are as follows: (1) determination of interrill contributions of different size fractions (five fractions are used in this study) using an improved interrill transport capacity formula, see equations (5), (6), (7a), and (7b); (2) determination of rill contributions and routing of the transported soil flux of different size fractions (both interrill and rill contributions) along the downslope, see equations (8), (9), (10a), and (10b); (3) updating the composition of the active layer based on the net fluxes of material of each size fraction, equation (11); and (4) aggregating the daily net fluxes to a monthly scale to estimate losses or gains in SOC stocks, see equations (12)–(17).

2.2.2.1. Size Fractions

We take advantage of existing WEPP features to represent size fractions of soil (denoted by p). WEPP employs five size fractions ($p = 1,\ldots, 5$) representing the soil matrix as both primary particles and aggregates [*Foster et al.*, 1985]. The primary particle diameters d_{clay}, d_{silt}, and d_{sand} are assigned median values of 0.002, 0.010,

and 0.2 mm, respectively. The diameter, d_{smag}, of small aggregates (mm) is approximated using the following empirical equations where *cl* denotes the clay percentage [*Foster et al.*, 1985]:

$$d_{smag} = \begin{cases} 0.030 & cl < 0.25 \\ 0.2(cl - 0.25) + 0.030 & 0.25 \le cl \le 0.60 \\ 0.100 & cl > 0.60 \end{cases} \quad (3)$$

For large aggregates, the diameter, d_{lgag} (mm), is determined as follows:

$$d_{lgag} = \begin{cases} 0.300 & cl \le 0.15 \\ 2cl & cl > 0.15 \end{cases} \quad (4)$$

In WEPP, small and large aggregates are assigned to specific gravity values of 1.8 and 1.6, respectively. If coarser material fractions were present, WEPP can easily incorporate them by modifying the number of soil size fractions *p*.

2.2.2.2. Interrill Erosion

For each size fraction *p*, the interrill detachment rate, $D_{\text{inte } p_i}$ (g/s/m), is estimated as:

$$D_{\text{inte } p_i} = f_p D_{\text{inte}_i} \quad (5)$$

where f_p is the mass fraction of size fraction *p* in the active layer and D_{inte} (g/s/m) is calculated as $D_{\text{inte}_i} = K_{int_i} I_e \sigma_{int_i} R_{int_i}$ [*Foster et al.*, 1995] where K_{int_i} is the interrill erodibility (g/s/m^4); I_e is the effective rainfall intensity (m/s); σ_{int_i} is the interrill runoff rate (m/s); and R_{int_i} is the width of the interrill area.

To estimate soil contributions to rills from interrill areas, we introduce into the ER module the *Abrahams et al.* [2001] transport capacity formula, rewritten for each size fraction as follows:

$$TC_{intp_i} = \phi \rho_{sp} \left[g \left(SG_p - 1 \right) d_p \right]^{0.5} d_p \quad (6)$$

where

$$\phi = a \tau^*_{int\ p_i} 1.5 \left(1 - \frac{\tau^*_{c\ int\ p_i}}{\tau^*_{int\ p_i}} \right)^{0.5} \left(\frac{u_{int_i}}{u*_{int_i}} \right)^{c} \left(\frac{w_{sp}}{u*_{int_i}} \right)^{-0.5}$$

$$a = 10^{-\ 0.42 Cr_{\text{int}_i} / Dr^{0.2}_{\text{int}_i}}$$

$$c = 1 + 0.42 Cr_{\text{int}_i} / Dr^{0.2}_{\text{int}_i}$$

where TC_{intp_i} (g/s/m) is the sediment transport capacity of size fraction *p* in the CV; SG_p is the particle specific gravity (−) of each size fraction *p*; ρ_{sp} is the particle density (g/m^3); d_p is the median particle diameter (m) for each fraction *p*; $\tau^*_{int\ p_i}$ is the dimensionless shear stress acting on size fraction *p* (−); $\tau^*_{c\ int\ p_i}$ is the dimensionless critical shear stress (−); u_{int_i} is the interrill flow velocity (m/s); $u*_{int_i}$ is the shear velocity (m/s); w_{sp} is the settling velocity (m/s) of the median particle diameter; and *a* and *c* are regression coefficients dependent on the concentration of roughness elements; Cr_{int_i} (−), and the characteristic roughness diameter, Dr_{int_i} (m) in the CV.

If the transport capacity of the size fraction, TC_{intp_i}, is greater than its detachment rate, (i.e., $TC_{intp_i} > D_{inte\ p_i}$), then the interrill supply, D_{intp_i}, of the size fraction to the rill (per unit rill area; kg/s/m^2) is determined as follows:

$$D_{intp_i} = \frac{D_{inte\ p_i}}{w_{rill}} \quad (7a)$$

where w_{rill} is the width of the rill (m). On the other hand, if $TC_{int\ p_i} < D_{inte\ p_i}$, then D_{intp_i} (g/s/m^2) is calculated as follows:

$$D_{int\ p_i} = \frac{1}{w_{rill}} \left[D_{inte\ p_i} - \frac{\beta w_{sp}}{\sigma_{\text{int}_i}} \left(D_{inte\ p_i} - TC_{int\ p_i} \right) \right] \quad (7b)$$

where β is a turbulence resuspension coefficient (assigned a value of 0.5) and w_{sp} is the settling velocity for size fraction *p* (m/s) estimated using the approach described in *Fox and Papanicolaou* [2007].

2.2.2.3. Rill Erosion and Downslope Particle Transport

A steady state form of the 1-D sediment continuity equation is used to account for the collective net fluxes contributed in the downslope by the interrill and rill areas. The downslope flux equation for each size

fraction is solved along a rill where the contributions of interrill areas are assumed to occur laterally along the rill longitude:

$$G_{ACTp,i} = D_{int\ p_i} + D_{rill\ p_i} \tag{8}$$

where G_{ACTp} (g/m/s) is the transported soil load of size fraction p derived from the active layer within CV i; (,) implies the derivative of G_{ACTp} in the downslope; D_{intp_i} is the net interrill flux rate of size fraction p (g/s/m^2) determined with equations (7a) and (7b); and $D_{rill\ p_i}$ is the net rill flux rate of size fraction p (g/s/m^2).

For determining whether net erosion or deposition is occurring within CV i, the rill flow transport capacity, $TC_{rill\ p_i}$ (g/m/s), is determined using the *Yalin* [1977] formula:

$$\frac{TC_{rill\ p_i}}{SG_p d_p \rho^{0.5} {\tau_{o\ rill\ p_i}}^{0.5}} = 0.635\delta\left[1 - \frac{1}{\beta_0}\ln(1+\beta_0)\right] \tag{9}$$

where

$$\beta_0 = 2.45\left(SG_p\right)^{-0.4}\left(\tau^*_{c\ rill\ p_i}\right)^{0.5}\delta$$

$$\delta = \frac{\tau^*_{rill\ p_i}}{\tau^*_{c\ rill\ p_i}} - 1$$

$$\tau^*_{rill\ p_i} = \frac{\tau_{o\ rill\ p_i}}{\rho\left(SG_p - 1\right)g d_p}$$

$$\tau^*_{c\ rill\ p_i} = \frac{\tau_{c\ rill\ p_i}}{\rho\left(SG_p - 1\right)g d_p}$$

where SG_p is the particle specific gravity (−) of size fraction p; g is the acceleration due to gravity (m/s^2); ρ is the density of water (g/m^3); d_p is the particle diameter (m) of size fraction p; $\tau_{o\ rill\ p_i}$ is the hydraulic shear stress (Pa); $\tau_{c\ rill\ p_i}$ is the critical erosional strength (Pa); $\tau^*_{\text{rill}\ p_i}$ denotes the dimensionless shear stress acting on the rill bed; $\tau^*_{c\ rill\ p_i}$ denotes the dimensionless critical shear stress (−), and β_0 and δ are dimensionless parameters that reflect the soil properties [*Foster and Meyer*, 1972; *Alonso et al*., 1981; *Finkner et al*., 1989].

When net erosion occurs for a size fraction (i.e., $TC_{rill\ p_i} > G_{ACTp_i}$) the rill erosion rate, $D_{rill\ p_i}$ (kg/s/m^2), is determined as follows:

$$D_{rill\ p_i} = K_{rill\ p_i}\left(\tau_{o\ rill\ p_i} - \tau_{c\ rill\ p_i}\right)\left(1 - \frac{G_{ACTp_i}}{TC_{rill\ p_i}}\right) \tag{10a}$$

where $K_{rill\ p_i}$ denotes the rill erodibility (s/m) that is a function of surface roughness and soil textural properties. When there is net deposition (i.e., $TC_{rill\ p_i} < G_{\text{ACT}p_i}$, $D_{\text{rill}\ p_i}$) is determined as follows:

$$D_{rill\ p_i} = \frac{\chi w_{sp}}{q_{rill\ i}}\left(TC_{rill\ p_i} - G_{\text{ACT}p_i}\right) \tag{10b}$$

where $q_{rill\ i}$ is the unit discharge (m^2/s) in the rill; w_{sp} is the settling velocity; and χ (~0.5) is a raindrop-induced turbulent coefficient [*Lindley et al*., 1995].

2.2.2.4. Active Layer Composition Updates

Equations (5) to (10a) and (10b) are solved for each size fraction to accommodate textural changes in the soil active layer in CENTURY. At the end of each time step, the updated mass fraction, $f^{j+1}_{\text{ACT}pi}$, of each size fraction p in the soil active layer of CV i at time j+1 is determined as follows [*Papanicolaou et al*., 2010]:

$$f^{j+1}_{ACTpi} = \frac{Mass^{j+1}_{\text{ACT}pi}}{\sum_p Mass^{j+1}_{\text{ACT}pi}} \tag{11}$$

where

$$Mass^{j+1}_{\text{ACT}pi} = Mass^{j}_{\text{ACT}pi} - \left(Mass^{j}_{\text{erod}pi} - Mass^{j}_{\text{depo}pi}\right) \pm A_{\text{CV}i} DZ \rho_{si} f_{PARpi}$$

where $Mass^{j}_{ACTpi}$ is the mass with size fraction p in the active layer at time j (g); $Mass_{\text{erod}pi}$ is the mass with size fraction p (g) that eroded within time interval DT; $Mass_{\text{depo}pi}$ is the deposited mass with size fraction p (g)

within DT; A_{CVi} is the surface cross-sectional area (m^2) of CV i; f_{PARpi} is the mass fraction of size fraction p transferred to (− under net deposition) or incorporated from the parent layer (+ under net erosion); ρ_{si} is the bulk density of the parent layer (under net erosion) or the active layer (under net deposition); and DZ_i is the net change in bed elevation (m) for CV i accounting for the net flux of material for all size fractions and the soil porosity.

2.2.2.5. Soil Enrichment and ER Determination

We determine the ER of mobilized and deposited soil in the CVs by determining the specific surface area of the active soil material as follows:

$$SSA = \sum_p f_{mp}\left(\frac{fr_{sndp}SSA_{snd} + fr_{sltp}SSA_{slt} + fr_{clyp}SSA_{cly}}{1 + fr_{orgp}} + \frac{fr_{orgp}SSA_{org}}{1.73}\right) \tag{12}$$

where f_{mp} is the proportion of size fraction p in the material being considered (i.e., active layer, mobilized or deposited material); fr_{sndp}, fr_{sltp}, fr_{clyp}, and fr_{orgp} are the mass proportions of sand, silt, clay and organic matter in each size fraction p, respectively; and SSA_{snd}, SSA_{slt}, SSA_{cly}, and SSA_{org} are the specific surface areas of sand, silt, clay and organic carbon, respectively, taken as 0.05, 4.0, 20, and 1000 m^2/g, respectively [*Sposito*, 1989; *Flanagan and Nearing*, 2000]. For in situ soils, f_{mp} is the proportion of size fraction p in the soil active layer, whereas for mobilized and deposited soils, f_{mp} is the proportion of size fraction p in the total eroded and deposited soil fluxes, respectively. The value 1.73 is used to convert the fraction of organic matter to organic carbon [e.g., *Neitsch et al*., 2002].

The capacity of a soil particle to bind SOC is proportional to the particles surface area [*Palis et al*., 1997; *Wang et al*., 2013], and the soil enrichment ratio of CV i at time j, $(ER_{\text{Erod ACT}})_i^j$, (assumption 5) can be expressed as follows:

$$(ER_{\text{Erod ACT}})_i^j = \left(\frac{SSA_{\text{Erod}_{\text{ACT}}}}{SSA_{\text{SOIL}_{\text{ACT}}}}\right)_i^j \tag{13}$$

where $SSA_{\text{Erod}_{\text{ACT}}}$ is the specific surface area of eroded soil (m^2/g); and $SSA_{\text{SOIL}_{\text{ACT}}}$ is the specific surface area of the in situ soil (m^2/g). To determine the enrichment of the material being deposited within CV i at time j, $\left(ER_{\text{Depo}_{\text{ACT}}}\right)_i^j$ the following expression is used:

$$\left(ER_{\text{Depo}_{\text{ACT}}}\right)_i^j = \left(\frac{SSA_{\text{Depo}_{\text{ACT}}}}{SSA_{\text{Mob}_{\text{ACT}}}}\right)_i^j \tag{14}$$

where $SSA_{\text{Depo}_{\text{ACT}}}$ is the specific surface area of deposited soil (m^2/g) and $SSA_{\text{Mob}_{\text{ACT}}}$ is the specific surface area of the total mobilized soil from which material is deposited (m^2/g).

2.2.2.6. Net SOC Fluxes Within the Soil Profile

The net flux of material, $(G_{\text{ACT}})_i^j$ in g/s, from CV i at time j is calculated as the sum of the fluxes of all the size fractions (i.e., $(G_{\text{ACT}})_i^j = \sum_p \left(G_{\text{ACT}p} \times w_{rill}\right)_i^j$). The calculated $(G_{\text{ACT}})_i^j$ values are aggregated for each month to estimate the loss or gain in SOC for the month. For net erosional events (i.e., $G_{\text{ACT}} > 0$), the loss of SOC for CV i in a given month j, $(SOC_{\text{NetErod}_{\text{ACT}}})_i^j$, is estimated as follows:

$$(SOC_{\text{NetErod}_{\text{ACT}}})_i^j = (SOC_{\text{ACT}})_i^j \left(\frac{G_{\text{ACT}} ER_{\text{Erod ACT}}}{\rho_{\text{Bulk}_{\text{ACT}}} D_{\text{ACT}}}\right)_i^j DT \tag{15}$$

where $\rho_{\text{Bulk}_{\text{ACT}}}$ is obtained from equation (2); and ER_{ErodACT} is the enrichment ratio of monthly-aggregated material leaving the CV (see equation (13)).

Per assumption 3, the portion of $(SOC_{\text{NetErod}_{\text{ACT}}})_i^j$ that is considered to be mineralized during transport, $(SOC_{\text{OX}_{\text{ACT}}})_i^j$, is estimated as follows:

$$(SOC_{\text{OX}_{\text{ACT}}})_i^j = f_{\text{OX}_i} (SOC_{\text{NetErod}_{\text{ACT}}})_i^j \tag{16}$$

where f_{OX_i} is a fixed fraction assumed to be 20% [*Yadav and Malanson*, 2009] in this study. For net depositional events ($G_{\text{ACT}} < 0$), fluxes of SOC being deposited within CV i in month j, $\left(SOC_{\text{NetDepo}_{\text{ACT}}}\right)_i^j$ are expressed as follows:

$$\left(SOC_{\text{NetDepo}_{\text{ACT}}}\right)_i^j = (1 - f_{\text{OX}i-1})(SOC_{\text{NetErod}_{\text{ACT}}})_{i-1}^j \frac{(G_{\text{ACT}})_i^j}{(G_{\text{ACT}})_{i-1}^j} \left(ER_{\text{Depo}_{\text{ACT}}}\right)_i^j \tag{17}$$

Table 1. Summary of Local Historic Management Practices Used in Model Simulations[a]

Time Period	Management	Rotation (year)	Crop	Tillage	Fertilizer
1930–1975	C-C-O-M-M	1	Corn	MP	Manure,
	(Diversity)	2	Corn	MP	Inorganic
		3	Oats	–	
		4	Alfalfa	–	
		5	Alfalfa	–	
1976–1990	C-C-B	1	Corn	CP	Broadcast
	(Intensification)	2	Corn	CP	Urea
		3	Soybean	CP	
1991–2010	STC-NTB	1	Corn	FC	Anhydrous
	(Conservation)	2	Soybean	–	Ammonium

[a]MP, moldboard plow; CP, chisel plow; FC, field cultivator.

where $(SOC_{\mathrm{NetErod_{ACT}}})_{i-1}^{j}$ is the stock of SOC entering CV *i* from the upslope; and $\left(ER_{\mathrm{Depo_{ACT}}}\right)_i^j$ is the enrichment ratio of monthly-aggregated material being deposited within CV *i* (see equation (14)).

2.2.3. Updating SOC Stocks

Using the above outputs from WEPP and the ER module as inputs to the CENTURY model, CENTURY is run sequentially for each CV along the downslope, simulating SOC dynamics from the impact of management and climatic events. Stocks of available SOC within the soil active layer are first determined (equation (1)).

At the end of each month *j*, the net change in total SOC in the soil active layer of CV *i*, $(\Delta SOC_{\mathrm{ACT}})_i^j$, in g C/m^2, is calculated as follows based on inputs from equations (15) and (17).

For net erosion,

$$(\Delta SOC_{\mathrm{ACT}})_i^j = (SOC_{\mathrm{ACT}})_i^j - (SOC_{\mathrm{ACT}})_i^{j-1} \cong (STAB_{\mathrm{ResD_{ACT}}} - R_{\mathrm{HetSOC_{ACT}}} - SOC_{\mathrm{NetErod_{ACT}}})_i^{j-1} \quad (18a)$$

For net deposition,

$$(\Delta SOC_{ACT})_i^j = (SOC_{ACT})_i^j - (SOC_{ACT})_i^{j-1} \cong \left(STAB_{ResD_{ACT}} - R_{HetSOC_{ACT}} + SOC_{NetDepo_{ACT}}\right)_i^{j-1} \quad (18b)$$

where $STAB_{\mathrm{ResD_{ACT}}}$ is the net amount of SOC that was stabilized from decayed residue and root stocks for the month (g C/m^2; assumption 8; see Appendix A for more detail); and $R_{\mathrm{HetSOC_{ACT}}}$ is the heterotrophic soil respiration during SOC decomposition for the month (g C/m^2; see Appendix A for more detail).

3. Study Site Characteristics

3.1. Topographic Characteristics

The representative hillslope selected here is located within a region of the Clear Creek watershed where the predominant soil series is Tama (fine-silty, mixed, superactive, mesic Typic Argiudoll), a mollisol, or prairie-derived soil, that is well drained and formed from loess [*Bettis et al.*, 2003]. Since European settlement, over 80% of the watershed has been converted from intrinsic prairie conditions to row crop agriculture.

Although the watershed features a mosaic of convex and concave hillslopes [*Dermisis et al.*, 2010], the selected representative hillslope has a convex, downslope curvature as it represents the worst-case scenario in terms of soil and SOC loss [e.g., *Huang et al.*, 2002; *Rieke-Zapp and Nearing*, 2005; *Hancock et al.*, 2010; *Dermisis et al.*, 2010]. The representative hillslope has an elevation drop of 22.5 m along a downslope length of 430 m yielding a declination of 5%, which is the approximate average gradient for the watershed [*Dermisis et al.*, 2010].

For the case study, both upslope and downslope zones (CVs) have the same soil series, which is Tama. The representative hillslope does not extend all the way to the floodplain where the dominant soil series is Colo. The length and average gradient of the upslope were 320 m and 5.8%, respectively, and of the downslope, 110 m and 3.5%, respectively.

3.2. Management Practices

A detailed time series of local, historical management practices is provided in Table 1. The first cultivation practices were introduced around 1930 following a final burn and intensive breakup of prairie sod with

the moldboard plow [*Hart*, 2001]. A 5 year diverse crop rotation of corn-corn-oat-meadow-meadow (CCOMM) with organic fertilizer was then adopted. In years 1 and 2 of that rotation, corn (*Zea mays*) was planted and the moldboard plow was used for both spring and fall tillage. Oats (*Avena sativa*) and alfalfa (*Medicago sativa*) were planted simultaneously in year 3 of the rotation with the oats acting as a companion crop to protect the alfalfa from excessive sunlight exposure and weed competition. Grain harvest of the oats was performed in late summer of year 3 while in years 4 and 5, the alfalfa was cut and baled for hay twice per year. In each year of this 5 year rotation, manure applications were applied in both spring and fall. However, in 1951, these manure applications were replaced with inorganic fertilizers [*Keeney and Hatfield*, 2008].

During the early 1970s, grain prices and demand began to surge, which prompted shifts of many biodiverse crop rotations (e.g., CCOMM) to more intensified production of other commodity crops [*Rupnow and Knox*, 1975; *Trautmann et al*., 1985]. From 1976–1990, soybeans (*Glycine max*) replaced oats and alfalfa grasses in a 3 year rotation of corn-corn-beans, CCB. The CCB management period consisted of larger fertilizer applications and higher tillage intensity with the use of the chisel plow [*Reicosky et al*., 1995; *Keeney and Hatfield*, 2008].

In the 1990s, intensified practices were replaced with more conservative tillage practices, including the 2 year corn-soybean rotation of spring till corn/no-till bean, STC-NTB [*Abaci and Papanicolaou*, 2009]. During corn production in the first year of the rotation, a field cultivator performed reduced spring tillage prior to planting. In the second year of the rotation, soybeans were planted under no-till conditions, with only minor disturbances to the soil from ripple coulters to chop up and remove residue stubble when planting. Fertilizer applications of anhydrous ammonium were knifed into the soil following soybean harvest when soil conditions were favorable [*Keeney and Hatfield*, 2008].

3.3. Climatic Conditions

Due to the midcontinental location of Iowa, the climate for Clear Creek is characterized by hot summers, cold winters, and wet springs [*Highland and Dideriksen*, 1967]. Daily high temperatures reach an average July maximum of 30 °C, while daily low temperatures reach an average minimum of −10°C in February [*Markstrom et al*., 2012]. Average annual precipitation is approximately 876 mm/yr with convective thunderstorms prominent in the early summer and snowfall in the winter [*Iowa Environmental Mesonet (IEM)*, 2015]. For site-specific information, the observed data from a neighboring weather station found in Williamsburg, IA was used [*Arnold and Williams*, 1989; *Gete et al*., 1999; *Abaci and Papanicolaou*, 2009]. We focus on the period of 1930–2010 as this is the period coinciding with the different management periods described earlier (see Table 1).

The time series of historic monthly precipitation for the period of 1930–2010 highlights a sequence of seasonal Gaussian distributions, with the peak rainfall in the watershed being received in May and June of each year [*Abaci and Papanicolaou*, 2009]. In addition to the seasonal variability, several notable extreme climatic events, namely, floods and droughts have occurred throughout this time period, with implications to the overall carbon cycle [*Reichstein et al*., 2013]. Two major flooding events occurred in years 1982 and 1993 [*Heinitz*, 1986; *Mutel*, 2010] and an intensive drought period in 1988 [*Handler*, 1990].

4. Methodological Procedures

4.1. Model Initialization and Calibration

Prior to performing model simulations, the initialization and calibration steps of the loosely coupled models were considered carefully. Careful attention was first placed on the initialization of CENTURY to ensure that the initial stocks of SOC adequately represented the conditions found within the active layer (top 20 cm) before introducing cultivation practices. The model was run for an extended period of time prior to 1930 to allow key biogeochemical processes and recalcitrant pools of SOC within CENTURY sufficient time to reach the *pseudoequilibrated state* conditions where conditions do not change in an average sense with time [*Metherell et al*., 1993]. The year 1930 is considered a benchmark date to our modeling efforts as this is the year that the first cultivation practices were introduced.

Calibration was needed for both models. Topographic data (section 3.1) as well as longitudinal data of changes in management practices (section 3.2) and climate records (section 3.3) helped us perform the calibration procedures. Appendix A provides details of the initialization and calibration steps.

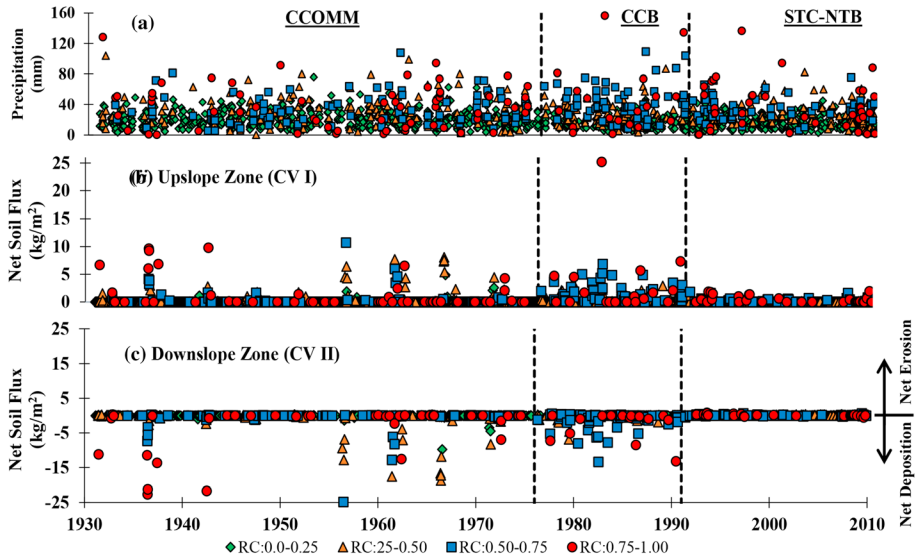

Figure 4. Time series of simulated runoff coefficient and soil redistribution. (a) A time series of simulated runoff coefficients (RC) is shown, with corresponding net erosion rates for the (b) upslope and (c) downslope zones of the representative hillslope. The net erosion plots (Figures 4b and 4c) are color coded with the following corresponding RC intervals (0.00–0.25 = green diamond; 0.25–0.50 = orange triangle; 0.50–0.75 = blue square; 0.75–1.00 = red circle). The time series covers the years 1930 to 2010, reflecting CCOMM, CCB, and STC-NTB management practices. Note that the scale of net erosion for the downslope zone is different from the upslope zone due to the presence of net deposition.

4.2. Verification

To assess the predictive capabilities of the newly developed framework, samples ($n = 250$) were collected from representative field locations in 2005, 2007, and 2010 and tested for SOC using an elemental analyzer following methods in *Martinotti et al*. [1997] and *Pansu et al*. [2001]. Sampling locations were determined based on results from *Papanicolaou et al*. [2009] and literature found in *Fox and Papanicolaou* [2007, 2008]. Factors hypothesized to induce variation of SOC stocks in the study site (e.g., depth, soil type, management, and gradient) were used to fine tune the sampling locations in both eroding and depositional areas. Comparisons of the measured and the simulated values are presented in section 5.4.

5. Analysis of Results

In this section, we present estimates of net erosion/deposition and dry soil bulk density generated from WEPP, as well as ER values generated from the ER module for the upslope and downslope CVs for the period of 1930–2010. These estimates are generated by accounting for rill and interrill contributions and are utilized to generate, via CENTURY, SOC trends where long-term changes in SOC stocks are assessed as a function of historic management practices and climatic conditions for 1930–2010.

5.1. Spatial Heterogeneity and Temporal Variability Results of Net Soil Fluxes

Figure 4a provides a time series of the daily precipitation, color coded with simulated daily runoff coefficients (RC) from 1930–2010 to discern the effects of rainsplash from concentrated flow on the magnitude and direction of the soil fluxes. Figures 4b and 4c illustrate the corresponding net erosion and net deposition fluxes for the different management practices.

The RC values throughout the CCOMM management period (1930–1975) averaged 0.18. During the corn production years of the CCOMM rotation (years 1–2), however, RC values were found to be 35% higher than years in grass production (years 3–5 of rotation) despite similar precipitation amounts. During the CCB management period (1976–1990), RCs were highest, averaging 0.30. The highest RC during this time period was during the June flood of 1982 [*Heinitz*, 1986; *Barnes and Eash*, 1994], which produced a monthly RC value of 0.65. In the management period of STC-NTB (1991–2010), RC values dropped to an average of 0.26, as conservation tillage methods become prevalent. However, extreme events during the flood of 1993 had an average RC of 0.46, which was almost double the average of the entire period.

In CV I (Figure 4b), the net erosion events appeared to be more spread out during the CCOMM period comparatively to the CCB and STC-NTB periods. Significant erosion events occurred for the CCOMM period in only two of the 5 years of the rotation when corn was grown and attributed to the decreased land cover from tillage activities. The average net monthly erosion for the entire period was estimated as 0.48 kg/m^2/month. The frequency of erosion events intensified during the CCB period due to reduced land cover in each year of the rotation and increased tillage frequency (3 out of 3 year for CCB versus 2 out of 5 year for CCOMM). The first year of the rotation generally experienced the highest net erosion rates because fall tillage events performed after harvesting soybeans provided less residue cover than corn [*Abaci and Papanicolaou*, 2009]. The average net monthly erosion during the CCB management period was 0.99 kg/m^2/month, which was more than double the CCOMM rates. The largest net flux for the entire simulation period, 25.2 kg/m^2, occurred in the CCB period during the recorded flood event in June of 1982, where 15 cm of rainfall fell on top of an already wet year [*Barnes and Eash*, 1994]. There was a significant reduction in net erosion rates with the introduction of conservation practices in the STC-NTB period, in the form of reduced tillage and no-till practices [*Abaci and Papanicolaou*, 2009]. Overall, during STC-NTB management, the soil loss in CV I was found to average 0.21 kg/m^2/month, which was less than half the average rate during the CCOMM management. Similar value ranges for STC-NTB management have been reported in this region (although the emphasis has been in Western Iowa) by *Burkart et al*. [2005] and *Karlen et al*. [2013].

In the downslope control volume, CV II (Figure 4c), the absolute magnitude of net soil fluxes during all management periods was generally less than the magnitude in the upslope CV. During the CCOMM and CCB periods, deposition events in the downslope appeared to "mirror" incoming fluxes from the upslope (Figure 4b), suggesting that contributions from the upslope generally exceeded the transport capacity of flow in the downslope, where the unit flow power term—defined as the amount of flow energy available to mobilize and transport material [*Yang*, 1973] and expressed in equation (9) through the bed shear stress terms and coefficients as functions of gradient and velocity—was lower comparatively to the upslope. Overall, CV II experienced an average monthly net deposition rate of 0.66 kg/m^2/month in the CCOMM period. Net deposition events continued throughout the CCB management period, with an average net monthly deposition rate of 1.08 kg/m^2/month. This trend was consistent with net fluxes from the upslope during the CCB period being twice as much as the fluxes during the CCOMM period. During the STC-NTB conservation management, net soil fluxes in the downslope switched from net deposition to net erosion, at an average monthly rate of 0.11 kg/m^2/month. The considerably reduced supply of incoming material from the upslope during the STC-NTB period resulted to a supply limited system in CV II and increased mobilization of material derived from the downslope. Hence, although there were still some deposition for certain events, on average, the net flux for each month had generally a positive direction (net erosion). Despite the switch to net erosion, the flux rates in the downslope were less than half the rates in the upslope due to the lower unit stream power (equations (9), (10a), and (10b)). What is worth noting is that despite the positive net flux in both the upslope and downslope CVs for the STC-NTB period, the average monthly flux of material exiting the hillslope for that period was considerably less than the CCOMM and CCB periods due to the effectiveness of the STC-NTB management at reducing net erosion overall.

5.2. Bulk Density Spatial and Temporal Variability

As seen in Figure 5, the dry soil bulk density (BD) decreased directly following a tillage event and then increased as cumulative rainfall increased. The simulated BD values ranged between 0.92 to 1.40 g/cm^3. This is in good agreement with observed BD values of 0.90 to 1.40 g/cm^3, gathered from a collection of past and current research conducted within the study site [*O'neal*, 2009; *Papanicolaou et al*., 2015; http://critical-zone.org/iml/infrastructure/field-area/clear-creek-watershed].

The introduction of the moldboard plow spurred interannual fluctuations in BD, decreasing values from 1.40 to 0.92 g/cm^3 during the years in which corn was planted in the CCOMM management period. The BD increased in the months following the tillage events, potentially due to weight consolidation. In rotation years 3–5 when oats or alfalfa was present, the BD increased due to the prolonged absence of tillage events. During the CCB management period, interannual variability in BD decreased (1.35 to 1.00 g/cm^3) as less intensive tillage practices were used in the production of both corn and soybeans, and the BD was unable to reach to the maximum values found in CCOMM because the CCB rotation did not have long-enough "rebounding" periods. In year 1 of the 2 year STC-NTB management practice, fluctuations in BD ranged from

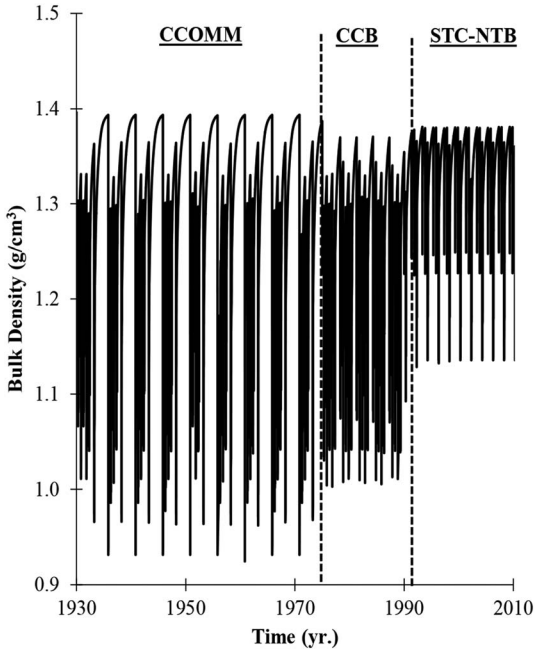

Figure 5. Soil bulk density. A time series of simulated daily soil bulk density values for the representative hillslope (black line) as determined by the WEPP model. The time series covers the period from 1930 to 2010 to reflect initiation of tillage. Field measurements of soil bulk density from the study watershed ranged from 0.90 to 1.48 g/cm^3, which are in good agreement with simulated values [*Papanicolaou et al.*, 2008; *O'Neal*, 2009].

1.38 to 1.13 g/cm^3. The smaller decrease in density was found to be from the reduced spring tillage before corn planting [*Abaci and Papanicolaou*, 2009]. However, in the second year of the rotation, when no-till was used for soybean production, the even smaller decrease in BD from 1.35 to 1.25 g/cm^3 was due to disturbance of the soil by the planter, which was less intrusive. At the end of the second year, application of the anhydrous also caused the BD to drop to 1.20 g/cm^3.

Overall, the approximate 20–40% change in BD supports the need to account for temporally updated values of BD in quantifying transport and deposition rates of soil and SOC. Similar trends and the need to account for the chronosequence in BD changes have been reported in the literature [*Lal*, 2005; *Kuhn et al.*, 2009; *Schwärzel et al.*, 2011; *Celik et al.*, 2012].

5.3. Enrichment Ratio Spatial and Temporal Variability

Figure 6 highlights the time series of simulated ER values for the representative hillslope from 1930–2010. Figures 6a and 6b represent material leaving the upslope and downslope CVs, respectively, while Figure 6c represents material being deposited within the downslope CV. In all plots, the ER values are categorized into four classes corresponding to those used for the precipitation and net erosion plots in Figure 4 based on the four RC classes. The plots reveal three key findings: (1) there are distinct differences in ER between the upslope and the downslope; (2) ER varies with event magnitude; and (3) management practices affect the ER.

In the upslope CV (Figure 6a), ER values ranged from 0.97 to 3.25 for all runoff-generating storms, with the maximum value reducing systematically from 3.25 to 1.2 from the smallest RC range (0.00–0.25) to the largest RC range (0.75–1.00). The minimum ER value, on the other hand, was similar for all RC ranges, falling between 0.97 and 0.98. Average ER values followed the same trend as the maximum values, also systematically decreasing from 1.27 to 1.00 from the smallest RC range to the largest RC range. The general reduction in ER with increasing RC supports the notion of less preferential mobilization of different size fractions at higher flows where general motion usually occurs [*Papanicolaou et al.*, 2004]. Under these high-flow conditions, the composition of the mobilized soil is similar to the composition of the in situ soil, resulting in little to no SOC enrichment of the transported soil. The results indicated that, on average, mobilized material during CCOMM period was 8% more enriched compared to the in situ soil, whereas material mobilized during the CCB and STC-NTB periods were only 1% more enriched.

In the downslope CV, the average ER values under net erosion conditions (Figure 6b) were generally lower in magnitude compared to their corresponding values in the upslope CV. Like the upslope, the average ER values in the downslope decreased systematically with increasing RC range from 1.17 to 0.99. The smaller ER values in the downslope compared to the upslope highlighted the importance of rainsplash in the selective transport of finer material on the upper sections of the hillslope [*Nadeu et al.*, 2011; *Hu et al.*, 2013]. On the lower hillslope sections, concentrated flow effects, which tended to mobilize all fractions, were dominant and overshadowed the effects of rainsplash, leading to the smaller ER values. In the downslope CV, the mobilized material during the CCOMM period was only 4% more enriched than the in situ soil, implying that the loss in SOC per unit mass of soil eroded was less in the downslope compared to the upslope (for the same initial SOC content).

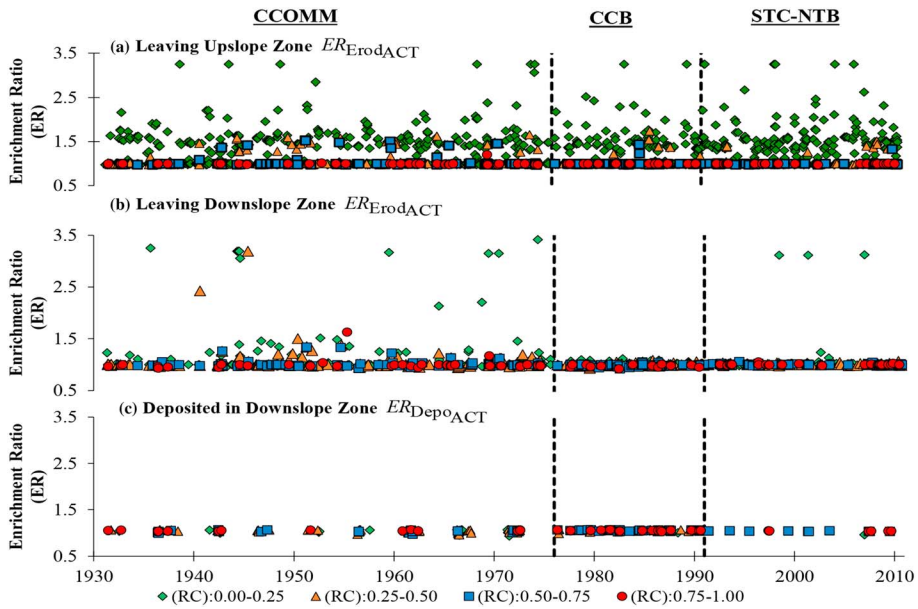

Figure 6. Time series of simulated enrichment ratios. A time series of daily simulated enrichment ratios (ER) values of material leaving the (a) upslope and (b) downslope zones of the representative hillslope are provided. (c) The ER values of the material being deposited within the downslope zone, aggregated to the monthly time scale. The ER values are broken into corresponding runoff coefficients (RC), with RC between 0.00 and 0.25 (green diamond); 0.25 and 0.50 (orange triangle); 0.50 and 0.75 (blue square); and 0.75 and 1.00 (red circle).

Under net deposition conditions (Figure 6c), material being transported from the upslope CV was deposited onto the active layer of the downslope CV. Deposition processes were also selective, but, on the contrary, favored heavier, generally larger size fractions. The deposited fraction was found to be either less or more enriched compared to the material being transported, depending on the composition of the deposited fractions. This is seen in Figure 6c, where the range of ER values (from equation (14)) falls between 0.93 and 1.07. The depositional patterns in Figure 6c reflect the management practices in each period. There are net deposition events during the two corn production years of the CCOMM period, net deposition events during each year of the CCB period, and net deposition events every other year of the STC-NTB period, reflecting the tillage practices adopted. The ER values for all the management periods suggest that, on average, depositional events resulted in the flux of material that was 3–5% more enriched into the soil. This is consistent with the deposition of larger size fractions containing finer enriched material in their composition [*Nadeu et al.*, 2011].

Overall, the smaller loss in SOC per unit mass of eroded soil in the downslope, combined with the relative enrichment of soil in the active layer, tended to promote higher SOC per unit mass in the downslope relative to the upslope. However, since the ER is concentration ratio, the actual loss or gain in SOC is dependent on the initial stocks of SOC to a large degree [*Schiettecatte et al.*, 2008].

5.4. Effects of Long-Term Changes in LULC on SOC Stocks

Figure 7 provides the time series of simulated monthly SOC stocks within the upslope and downslope CVs of the representative hillslope from 1930 to 2010. The year 1930 was selected to represent the introductory baseline SOC stock value of 4500 g C/m^2 supplied from the initialization (represented by the black dot in Figure 7) right before conversion to agricultural production.

In the upslope CV (green-colored line), the general trend includes (1) significant losses of SOC following conversion to row crop agriculture during the CCOMM period, (2) a "plateaued" recovery period during the CCB management period, and (3) a "rebounding" period during the implementation of current STC-NTB conservation practices. Similar trends have been reported in other assessments of SOC within IMLs [*Mann*, 1986; *Owens et al.*, 2002; *Liu et al.*, 2003; *Tornquist et al.*, 2009; *Brown et al.*, 2010; *Bortolon et al.*, 2011]. On conversion to row crop production in 1931, there was a sharp, initial spike in SOC stocks due the massive supply of

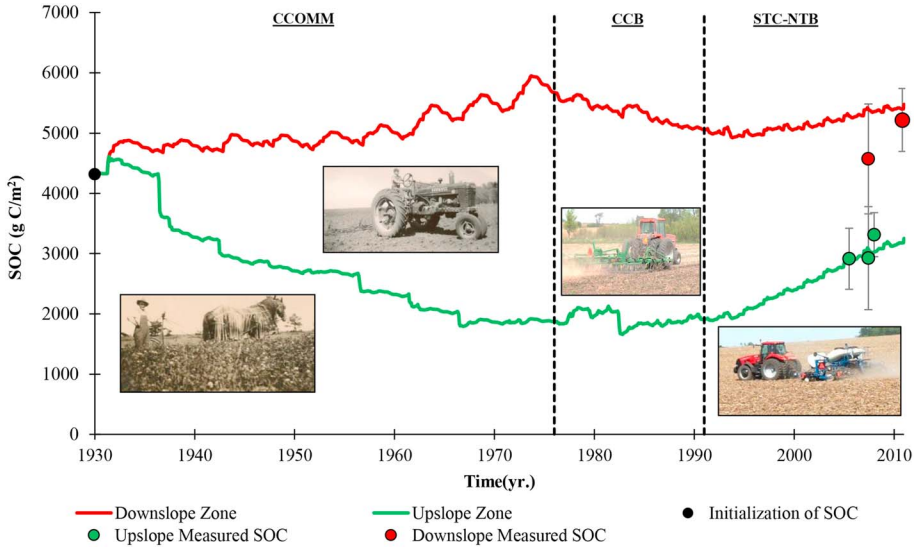

Figure 7. Spatial heterogeneity and temporal variability of SOC. A time series of simulated values of SOC is provided for the upslope (green line) and downslope (red line) zones of the representative hillslope, highlighting the variability of SOC throughout historic management practices from 1930 to 2010. Baseline stocks of SOC acquired during model initialization is plotted (black dot). In addition, field measured values of SOC collected within the upslope (green circle) and downslope (red circle) zones of several hillslopes within the study watershed are compared to corresponding simulated SOC values. Note: Vertical error bars represent the standard deviation of the samples in gC/m^2.

organic material delivered to the active layer through tillage-incorporation of prairie grasses. After the spiked flux, there were SOC losses attributed to the combined tillage effects with rainfall-runoff erosion events [*Stinner et al*., 1983; *Tivy*, 1990]. This is seen in Figure 7 with a series of "descending staircases" suggesting losses in SOC with time especially throughout the CCOMM period. Residue incorporation rates (i.e., SOC contributions from residue decomposition; see equations (18a), (18b), and (B3)) during the period averaged 127 g $C/m^2/yr$, while heterotrophic respiration and net erosional SOC losses were 115 and 67 g $C/m^2/yr$, respectively.

During the CCB management period, enhanced crop production rates from increased fertilizer usage and genetic seed advancements (see Figure C1) began to halt the downward trend of SOC stocks. Residue incorporation rates during this period increased to an average of 237 g $C/m^2/yr$, while heterotrophic respiration and net erosional losses rose to 131 and 104 g $C/m^2/yr$, respectively. Overall, SOC stocks kept nearly constant despite a punctuated loss of SOC during the 1982 flood event [*Barnes and Eash*, 1994].

During the STC-NTB management period, the implementation of conservation practices further decreased erosion rates, while the adoption of high-yield crop hybrids increased plant production such that residue incorporation was greater than the losses due to decomposition and erosion, resulting in SOC stock increases. Here residue inputs averaged 247 g $C/m^2/yr$, while respiration and erosional losses were 148 and 29 g $C/m^2/yr$. Loss of SOC due to erosion under STC-NTB was almost 4 times smaller than the previous CCB period. In fact, net erosion fluxes from flooding events in 1993 were "dampened" in part due to the protection offered by increased residue cover from conservation (reduced and no-till) practices [*Rhoton et al*., 2002]. Toward the end of the simulation, SOC stocks appear to approach a new equilibrium value [*Six et al*., 2002; *Stewart et al*., 2007], building at a rate of 71 g $C/m^2/yr$, which is comparable to increases reported by *Reicosky et al*. [1995].

SOC within the downslope net depositional CV (red colored line) for all periods was found to be much higher than the upslope net erosional CV, which has been reported in the literature [e.g., *Stavi and Lal*, 2011; *Du and Walling*, 2011; *Navas et al*., 2012; *Wang et al*., 2015]. Throughout the CCOMM period, the gradient of SOC stocks increased as the frequency of deposition events (Figure 4c) and production rates also increased starting in the late 1950s (see Figure C1). Residue incorporation rates during this period averaged 196 g $C/m^2/yr$, while heterotrophic respiration was 217 g $C/m^2/yr$. Both of these rates were more than double the values found in

the upslope. In addition, SOC losses due to erosion in the downslope were minimized, averaging around 4 g C/m^2/yr, which is over 10 times less than upslope losses. The average annual stock of SOC deposited from CV I contributions was 55 g C/m^2/yr. This finding could have major implications to the overall carbon budget of the system as most of the mobilized material was not actually exiting the hillslope.

During the CCB period, the downslope experienced a constant degradation in SOC stocks. Residue incorporation and heterotrophic respiration rates averaged 226 and 305 g C/m^2/yr, respectively. The rotational switch from grasses to soybean production not only decreased organic inputs (less biomass) into the soil but also enhanced microbial activity through increased tillage frequency [*Stinner et al*., 1983; *Tivy*, 1990]. Average SOC losses due to erosion increased to over twice the CCOMM rates at 12 g C/m^2/yr, while fluxes of deposited SOC from CV I contributions decreased to 50 g C/m^2/yr.

In the STC-NTB management period, the SOC stock began to slowly build and continued to rise, but at a slower rate than the corresponding period for the upslope. Residue inputs averaged 291 g C/m^2/yr, while respiration losses were 235 g C/m^2/yr. Erosional SOC losses in the downslope during this period, however, were the highest of all periods, matching rates in the upslope at 34 g C/m^2/yr. Deposition of SOC during this period was negligible due to the reasons outlined earlier (see section 5.1).

Lastly, Figure 7 also provides a comparison of simulated SOC stocks with field measured values of SOC from a field site in Clear Creek that exhibit nearly identical properties with those selected for the representative hillslope during the simulations (green dot represents values from upslope; red dot represents values from downslope). The figure shows good correspondence between the measured and the simulated values for the representative hillslope. Field values of SOC in the upslope and downslope zones are both increasing over time, with the downslope values higher than the upslope values, which is consistent with the simulation and literature reports [e.g., *Liu et al*., 2003].

6. Discussion and Conclusions

This paper offers an improved methodological framework to account for the collective effects of soil erosion on SOC redistribution in IMLs by spatially simulating the key processes described in Figure 1, taking into consideration monthly-aggregated changes in ER and BD. The framework loosely couples two established process-based models, WEPP and CENTURY, to incorporate the effects of the described landscape features on SOC stocks. A newly developed ER module is used to overcome some important limitations of WEPP by accounting for (1) textural updates of the active layer, (2) the enrichment of material being deposited on the hillslope, and (3) explicitly considering the effects of splash-driven interrill erosion on ER estimates.

The framework is applied in Clear Creek to a representative hillslope that is discretized into two CVs, namely, an upslope net erosional zone and a downslope net depositional zone, to simulate spatial and seasonal changes in SOC stocks due to historical long-term changes in LULC (Table 1). Figure 8 summarizes the simulation results, illustrating the effects of management practice and hillslope location on changes in net soil fluxes, ER, BD, and associated SOC stocks. In the figure, the hollow arrows represent net soil fluxes, where net erosional fluxes are oriented in the downslope direction and net depositional fluxes are oriented vertically downward into the soil active layer. The sizes of the arrows represent the relative magnitudes of the fluxes; larger arrows indicate greater fluxes (and vice versa). SOC symbols with an upward arrow represent gains in SOC stocks while a downward arrow represents loss in SOC stocks. For ER and BD, the sizes of the symbols represent the relative magnitudes of the quantities.

During the CCOMM and CCB management periods, erosion fluxes from the upslope were generally higher than erosion fluxes from the downslope due to a greater supply of material from the upslope to the downslope resulting in a reduced capacity of flow to mobilize material in the downslope. On the contrary, during the STC-NTB period, erosion fluxes from the upslope were lower than the fluxes from the downslope since the supply from the upslope was greatly reduced and the flow in the downslope had a higher capacity to mobilize material. The average deposition rate was largest during the CCB period due to the highest supply of material from the upslope, attributed to the greater tillage frequency and the lower soil cover. The deposition rate was smallest during the STC-NTB period due to the least supply of material from the upslope attributed to the effectiveness of conservation practices.

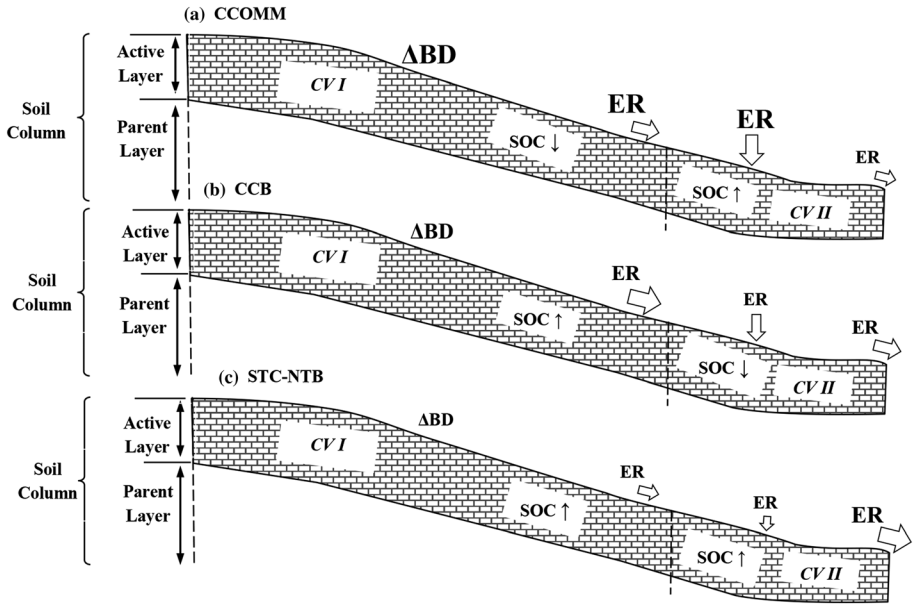

Figure 8. Summary of changes in net soil fluxes, BD, ER, and SOC with management practice and hillslope location. The arrows represent net soil fluxes, with erosional fluxes oriented in the downslope direction and depositional oriented vertically into the soil active layer. SOC, ΔBD, and ER symbols represent changes in SOC stocks, soil bulk densities, and enrichment ratios, respectively. The sizes of the arrows and symbols reflect the relative magnitudes of the quantities. For changes in SOC stocks, up arrows indicate gains in SOC while down arrows indicate SOC loss.

There was a clear distinction in simulated ER values between the upslope and the downslope. Net erosion fluxes exiting the upslope were consistently more enriched comparatively to net erosion fluxes from the downslope, suggesting that, under the same initial SOC stocks, SOC losses per unit eroded soil mass in the upslope would be greater than SOC losses per unit eroded soil mass in the downslope. The higher ER values in the upslope were attributed to the relatively more important role of rainsplash (associated with greater selective transport of finer material) on the upper sections of the hillslope comparatively to the lower sections, where concentrated flow effects were more important. Enrichment of eroded material was largest during the CCOMM period due to rainfall-runoff events with low runoff coefficients that preferentially transported finer fractions.

The simulations also highlighted the importance of accounting for the enrichment of the soil active layer in the downslope through the preferential deposition of larger size fractions containing finer enriched material in their composition. On average, deposited material was 3–5% more enriched than the mobilized material from where they deposited. Furthermore, the ER values of material eroded from the downslope were generally close to one as the dominant erosion processes and updated soil textures were such that mobilized material was just as enriched as soil in the active layer. This finding has implications on the fraction of the enriched organic carbon material that gets delivered into the stream under different management practices [*Dalzell et al*., 2007].

The fluctuations in BD were greatest during the first 2 years of the CCOMM rotation due to the use of the moldboard plow, which was the most intrusive tillage implement. The lowest BD fluctuations were observed during the STC-NTB due to the conservation practices adopted. Overall, the changes in BD during the simulation ranged between 20–40%, supporting the need to account for temporally updated values of BD in quantifying SOC fluxes.

The trends in SOC stocks differed between hillslope locations. In the upslope, SOC stocks declined during the CCOMM period due to intrusive tillage activities and high-erosion rates but increased during the CCB and STC-NTB periods. The increase during the CCB period despite the highest erosion rates was due to enhanced crop production rates from increased fertilizer usage and genetic seed advancements. The continued increase during the STC-NTB period was also due to the lower erosion rates stemming from conservation tillage practices. In the downslope, SOC stocks increased during the CCOMM period due to net deposition

and increased crop production. During the CCB period, however, the stocks decreased despite the high deposition rates due to reduced organic inputs from soybean and increased heterotrophic respiration from increased tillage frequency. SOC stocks increased during the STC-NTB period despite the greater erosion rates from the zone due to reduced heterotrophic respiration rates from conservation tillage and increased crop production rates.

Overall, the simulated SOC trends were in agreement with measured trends and values from a field site in Clear Creek that exhibited nearly identical properties with those of the representative hillslope used for the simulations (Figure 7). The field values of SOC in the upslope and downslope are both increasing over time, with the downslope values higher than the upslope values, which is consistent with the simulation results and literature reports [e.g., *Liu et al*., 2003; *Wang et al*., 2015].

As with any framework, there are some caveats associated to the approach considered herein. First, in our analysis we assumed that the soil composition of the active layer in 1930s is similar to the composition of the current active layer. This may not be the case in certain regions of the under investigation watershed where significant soil degradation may have occurred yielding the removal of the A horizon. A recent hydropedologic study by *Papanicolaou et al*. [2015] has shown that the steeper areas in Clear Creek with gradients higher than 5% may experience significant degradation resulting in significant coarsening of the top soil.

Second, the framework considers fixed size fractions estimated from empirical relationships developed by *Foster et al*. [1985]. For our site, this produced size fractions with median diameters ranging from 0.002 to 0.48 mm. In reality, however, there may be larger size fractions or aggregates enriched in SOC [*Di Stefano and Ferro*, 2002; *Zheng et al*., 2012] whose mobilization and deposition could impact SOC dynamics on the hillslope as they offer further protection to the organic matter trapped within their structure [*Berhe et al*., 2012]. Furthermore, it is assumed that the median diameters of the size fractions do not change under either the impact of rainsplash or hydraulic shear, or as they travel downslope. This may not be the case, as mobilized fractions may break down or grow in size due to mechanical, chemical, or biological processes.

Third, it is assumed that a fixed fraction (20%) of the mobilized SOC is oxidized during transport. However, according to *Lal* [2006], the actual magnitude of oxidation may be dependent on the composition of the organic matter. Uncertainty in the estimate is reflected in the broad range of fractions proposed in the literature [e.g., *Beyer et al*., 1993; *Lal*, 1995; *Schlesinger*, 1990; *Jacinthe and Lal*, 2001; *Smith et al*., 2001].

Fourth, the framework also adopts the concept of flow transport capacity which is embedded in WEPP as a means of determining whether or not net erosion or net deposition occurs. Under net erosion, the framework assumes that there is no deposition, whereas under net deposition, it assumes that there is no erosion. However, in nature, erosional and depositional processes occur simultaneously and so the soil active layer continually loses and gains SOC during rainfall-runoff events in both erosional (upslope) and depositional (downslope) zones [*Cao et al*., 2012]. This effect may be particularly important in the depositional zone, where material flux from the upslope could be deposited onto the active layer even when the transport capacity formula suggests that there should be net erosion.

Fifth, we assume that residue is uniformly distributed across the hillslope and does not simulate the mobilization and downslope transport of residue by runoff. The impact of residue redistribution on the landscape on SOC dynamics between the erosional and depositional zones is thus not accounted for [*Thompson et al*., 2008]. Lastly, the framework does not account for organo-mineral complexation phenomena, which appear to affect SOC storage differently in erosional and depositional zones [*Berhe et al*., 2012]. More research is however needed on this front to shed some light on the actual role that complexation plays in the persistence and storage of SOC in the two zones.

Overall, this study, although limited at the hillslope scale, offers some insight of what it will take in terms of human activity and here in terms of conservation practices to reverse further degradation of SOC. To assess the impact of management on SOC budgets at a larger scale where policy needs to be made (e.g., watershed), more detailed representation of the landscape and heterogeneous features present is needed [*Young et al*., 2014]. High-resolution elevation data, like repeated lidar, could be incorporated into future modeling efforts to identify flow pathways more precisely, as well as track the geomorphic evolution of the landscape stemming from a sequence of erosion or deposition events [*Young et al*., 2014]. In this case, flow pathways and connectivity of the landscape with neighboring units must be considered. Future research should more

explicitly account for the role of the drainage network on SOC storage as the eloquent work of *Liu et al*. [2011] has shown may play a significant role in SOC stocks as well as the role of exchanges between soil and atmosphere in IMLs.

Appendix A: Surface/Subsurface Flow Formulation

During a storm event, runoff is routed along the downslope of sequential control volumes (CVs) using the kinematic wave equation:

$$h_{i,j} + q_{i,i} = q_{li} \tag{A1a}$$

where i denotes space; the CV element i; j denotes time; (,) denotes first-order derivative; h is the flow depth (m) within CV i; q is volumetric flow discharge per unit width (m^2/s) in CV i; and q_l is a source term, a volumetric flow discharge, which incorporates the lateral (l) inflow rate of excess rainfall (m/s) to the CV, defined as follows:

$$q_{li} = r_i - f_i \tag{A1b}$$

where r is the rainfall rate (m/s); and f is soil infiltration rate (m/s). In equation (A1a), the left-hand side term q, is estimated using a typical power law, depth-discharge relation:

$$q = \alpha h^{3/2} \tag{A2}$$

where α is the kinematic depth-discharge coefficient determined as $\alpha = C\sqrt{S_o}$; C is the Chezy roughness coefficient; and S_o denotes the spatially average surface gradient of the CV. The infiltration rate of the active layer, f, in (equation (A1b)), is determined using the modified Green-Ampt equation to account for the effects of management and land use on flow partitioning through the inclusion of the effective hydraulic conductivity term:

$$f_i = F_{i,j} = \left(\frac{\Psi \vartheta_{di} + F_i}{F_i}\right) K_{ei} \tag{A3a}$$

where Ψ is the average capillary potential (m); ϑ_d is the soil moisture deficit (m/m); K_e is the effective hydraulic conductivity (m/s) that accounts for the collective effects of surface roughness and developed crust, tillage, raindrop impact, as well as canopy and residue cover within CV i [*Kidwell et al*., 1997]; and F is the cumulative infiltration depth (m), which is iteratively determined by applying the Newton–Raphson method to the equation:

$$F = K_e DT + \Psi \vartheta_d \ln\left(1 + \frac{F}{\Psi \vartheta_d}\right) \tag{A3b}$$

where DT is a time period (s). All terms in equations (B1)–(B3) are written for the CV element i.

Appendix B: SOC Decomposition Formulation

In CENTURY, the mass of SOC that is decomposed per unit area during a period DT, $D_{soc_{ACT}}$, and within the active layer (g C/m^2), or rate of decay, is approximated by a multiparametric equation [*Parton et al*., 2007] (assumption 3):

$$(D_{soc_{ACT}})_i^j = (SOC_{ACT})_i^{j-1} (K_{soc_{ACT}} ANERB_{ACT} CDI_{ACT} TEX_{ACT} TILL_{ACT})_i^{j-1} DT \tag{B1}$$

where $(SOC_{ACT})_i^{j-1}$ is the stock of SOC (g C/m) present within the active layer of CV i at time $j-1$, $K_{SOC_{ACT}}$ is the maximum, equilibrated SOC decomposition rate (one per year); $ANERB_{ACT}$ is a coefficient that adjusts $K_{SOC_{ACT}}$ due to anaerobic conditions and oxygen availability (−), which are dictated by the soil drainage, or downslope saturation; CDI_{ACT} the Climatic Decomposition Index, a correction coefficient that adjusts $K_{SOC_{ACT}}$ for seasonal changes in temperature moisture (−); TEX_{ACT} is a coefficient that accounts for soil texture effects on $K_{SOC_{ACT}}$ (−); and $TILL_{ACT}$ is a multiplier effect for enhanced $K_{SOC_{ACT}}$ following tillage under different management practices (−).

In a similar manner, the decomposition of residue, $D_{Res_{ACT}}$, within the active layer (g C/m^2) is expressed as follows:

$$(D_{Res_{ACT}})_i^j = (L_{ACT})_i^{j-1} (K_{Res_{ACT}} ANERB_{ACT} CDI_{ACT} TILL_{ACT})_i^{j-1} DT \tag{B2}$$

where L_{ACT} is the stock of soil residue within the active layer (g C/m^2); and $K_{Res_{ACT}}$ is the maximum, equilibrated residue decomposition rate (one per year).

A portion of the decayed stocks in equations (B1) and (B2) can be stabilized into more decay-resistant forms of SOC within the soil active layer based on soil texture, prevalent C/N ratio, and residue lignin content [*Sorensen*, 1981; *Van Veen et al*., 1984; *Holland and Coleman*, 1987]. The portion transferred to the more decay-resistant pools is what we define herein as "stabilized SOC" with the recognition though that this term has been presented in the literature in different ways somewhat inconsistent [*Berhe and Kleber*, 2013]. Taking into account these factors, the amount of SOC stabilized, $STAB_{SOC_{ACT}}$, in the active layer (g C/m^2) is expressed as follows (assumption 8):

$$(STAB_{SOC_{ACT}})_i^j = STAB_{SOCD_{ACT}} + STAB_{ResD_{ACT}} = f_{SOC}(D_{SOC_{ACT}})_i^j + f_{Res}(D_{Res_{ACT}})_i^j \quad \text{(B3)}$$

where f_{SOC} is the fraction of decomposed SOC that is stabilized (values found in *Parton et al*. [1987]); and f_{Res} is the fraction of decomposed residue that is stabilized as SOC based on lignin availability [*Melillo et al*., 1982]. Lastly, the portion of decayed stocks that is not stabilized within the soil is lost from the active layer in the form of CO_2, defined here as heterotrophic soil respiration (g C/m^2), $R_{Het_{ACT}}$, and expressed as follows:

$$(R_{Het_{ACT}})_i^j = R_{HetSOC_{ACT}} + R_{HetRes_{ACT}} = (1 - f_{SOC})(D_{SOC_{ACT}})_i^j + (1 - f_{Res})(D_{Res_{ACT}})_i^j \quad \text{(B4)}$$

Appendix C: Initialization and Calibration Steps

During the initialization period, intrinsic prairie conditions were considered, as a tall grass has been historically found throughout much of Iowa and the Midwest with minor grazing from free-range buffalo, and a 10 year fire frequency (Table C1) [*Hart*, 2001; *Weaver*, 1968; *Delucia et al*., 1992; *Macha and Cihacek*, 2009; *Kaiser*, 2011]. For the representative hillslope, an initial stock of SOC (at $t = 0$) was first estimated as 5500 g C/m^2 using the semiempirical relation developed by *Burke et al*. [1989], which considers average annual climatic and soil texture conditions as input parameters (see Table C1). Then, assuming the presence of the Big Bluestem (*Andropogon gerardii Vitman*), the model was run until the SOC stocks reached pseudoequilibrated values of 4520 g C/m^2 after approximately 4000 years. This pseudoequilibrated value of SOC agrees with the ranges of the reported field measured SOC stocks found within the Dinesen prairie, a remnant, native tallgrass prairie, the closest "undisturbed" location with SOC measurements to the study site [*Harden et al*., 1999; *Manies et al*., 2001]. No initialization of WEPP was needed since it was reasonable to assume that SOC mobilization due to erosion during the prairie period was insignificant other than some episodic events.

Typically, the calibration procedure for WEPP starts with flow (i.e., the driving mechanism for upland erosion) and continues with the sediment component [*Santhi et al*., 2001]. Additional information is needed in the model for key state variables such as the effective hydraulic conductivity, critical erosional strength, and residue cover, which is available for the study site [see *Abaci and Papanicolaou*, 2009, Tables 12 and 13]. Because

Table C1. Input Data for Model Initialization

Input Data	Units	Range	Reference
	Soil Properties		
Sand content	%	5.0–15.0	Current study
Silt content	%	60.0–70.0	Current study
Clay content	%	18.0–30.0	Current study
	Climate		
Monthly precipitation	(cm/month)	6.47–8.14	*Abaci and Papanicolaou* [2009]
Monthly temperature	(°C)	8.83–10.83	*IEM* [2015]
	Management-Prairie-Big Bluestem		
Lignin content		0.17	*Saxena and Stotzky* [2001]
Grazing frequency	(months/year)	2	*Hart* [2001]
Grazing intensity	% vegetation consumed	30	*Hart* [2001]
Fire frequency	# years without fire	10	*Collins and Wallace* [1990]
Fire intensity	% vegetation consumed	90	*Collins and Wallace* [1990]

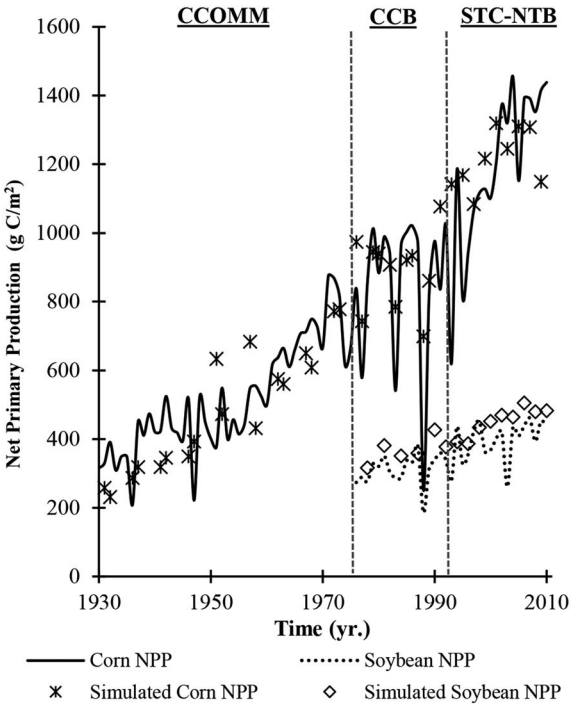

Figure C1. Model calibration. Local corn and soybean grain yield data and field measured values of vegetative carbon content as well as harvest indices were used to generate a times series of estimated aboveground net primary production (NPP) values of corn (solid black line) and soybeans (dashed black line) from 1930 to 2010 as well as simulated values of corn NPP (black cross) and soybean NPP (black diamond). The simulated values of NPP are the average of the upslope and downslope zones.

the procedural steps for calibrating WEPP have been extensively described in the literature [e.g., *Flanagan et al*., 2007; *Papanicolaou and Abaci*, 2008; *Abaci and Papanicolaou*, 2009; *Dermisis et al*., 2010] an emphasis here has been placed on the calibration for CENTURY.

The plant production submodel of CENTURY was calibrated to ensure accurate inputs of plant material into the soil active layer. Based on prior studies, the CENTURY model must be first calibrated using reported ranges of aboveground net primary production (NPP) in this region, defined here as the total net carbon stored in aboveground vegetation (i.e., stems, leaves, and grain) [e.g., *Chapin et al*., 2002]. Having the NPP estimated values within the measured ranges was deemed important for ensuring that CENTURY incorporates the correct inputs of aboveground C allocation for simulating belowground C allocations and stocks. The first step of the calibration process involved the collection of historic corn and soybean grain yield data (1930–2010) from Iowa County, where is the study location [*National Agricultural Statistics Service* (*NASS*), 2012]. Yield data were converted to total grain mass and corrected for seed moisture, which is commonly assumed to be 15.5% [*Lauer*, 2002]. Using unique harvest indices, defined here as the ratio of grain to total plant mass [*Huehn*, 1993; *Prince et al*., 2001], the grain mass was used to estimate aboveground biomass. The aboveground biomass and grain mass data were then converted to a carbon density, namely, NPP, by utilizing vegetative carbon contents of corn and soybean plants (i.e., leaves, stems, and grain) collected within the study site (A. N. Papanicolaou, unpublished data, 2014). Measured values of corn and soybean plant carbon contents were found to be in good agreement (correlation above 90%) with reported literature values [*Latshaw and Miller*, 1924; *Machinet et al*., 2009].

A sensitivity analysis revealed that precipitation and temperature data were sensitive parameters within the CENTURY plant production submodel [*Xiao et al*., 2004; *Schurgers et al*., 2011]. For this reason, local climate data from the Williamsburg site was used to simulate the time series of NPP from 1930–2010. The simulation period was partitioned into the following key crop rotations: CCOMM from 1930 to 1975; CCB 1976 to 1990; and STC-NTB 1991 to 2010 (see Table 1), with soybeans present in years 1976–2010, and corn present throughout the entire simulation. During the calibration efforts the reported statewide nitrogen fertilizer application rates for Iowa were adopted [*NASS*, 2012].

Comparisons of NPP values estimated using the above mentioned methods and simulated NPP from 1930 to 2010 are shown in Figure C1. In terms of corn, there is an overall upward trend in simulated NPP from 1930 to 2010 which agrees well with the estimated NPP values. During this time period, NPP increases from 350 g C/m^2 to around 1400 g C/m^2. Large variability in NPP occurs during CCB management, between the years 1980 to 1993, due to reported extreme climatic events, namely droughts and flooding [*Rosenzweig et al*., 2002].

For soybeans (1976–2010), simulated values increase from 288 g C/m^2 to around 450 g C/m^2. Overall, the simulated and estimated NPP appear to be in an agreement (R^2 value = 0.84) for the entire period from 1930 to 2010.

Acknowledgments
The modeling component of this research was supported by the National Science Foundation grant EAR1331906 for the Critical Zone Observatory for intensively managed landscapes (IML-CZO), a multiinstitutional collaborative effort. Additionally, this research was partially supported by the NASA EPSCoR Program (grant NNX10AN28A) and the Iowa Space Grant Consortium (grant NNX10AK63H) as well as the Leopold Center for Sustainable Agriculture grant XP2010-03 where data for model calibration and validation have been collected. The second author was partially supported by a Graduate Assistance in Areas of National Need (GAANN) fellowship grant and the University of Iowa NSF IGERT program, Geoinformatics for Environmental and Energy Modeling and Prediction. The authors would like to recognize the help of Cindy Keough from Natural Resources Ecology Laboratory-Colorado State University for technical advice in coupling the CENTURY model with WEPP. As always the authors would like to acknowledge the long-term partnership with the ARS lab at West Lafayette and Dennis Flanagan for working with different versions of the WEPP model. The data of this research are available to the interested reader upon written request to the first author.

References

Abaci, O., and A. N. Papanicolaou (2009), Long-term effects of management practices on water-driven soil erosion in an intense agricultural sub-watershed: Monitoring and modeling, *Hydrol. Process.*, *23*(19), 2818–2837.

Abrahams, A. D., G. Li, C. Krishnan, and J. F. Atkinson (2001), A sediment transport equation for interrill overland flow on rough surfaces, *Earth Surf. Processes Landforms*, *26*(13), 1443–1459.

Alonso, C. V., W. H. Neibling, and G. R. Foster (1981), Estimating sediment transport capacity in watershed modeling, *Trans. ASAE*, *24*(5), 1211–1220.

Andrews, S. S., J. P. Mitchell, R. Mancinelli, D. L. Larlen, T. K. Hartz, W. R. Horwarth, G. S. Pettygrove, K. M. Scow, and D. S. Munk (2002), On-farm assessment of soil quality in California's Central Valley, *Agron. J.*, *94*, 12–23.

Arnold, J. G., and J. R. Williams (1989), Stochastic generation of internal storm structure, *Trans. ASAE*, *32*(1), 161–166.

Barnes, K. K., and D. A. Eash (1994), Flood of June 17, 1990, in the Clear Creek basin, east-central Iowa US Geological Survey.

Berhe, A. A., and M. Kleber (2013), Erosion, deposition, and the persistence of soil organic matter: Mechanistic considerations and problems with terminology, *Earth Surf. Processes Landforms*, *38*(8), 908–912.

Berhe, A., J. W. Harden, M. S. Torn, M. Kleber, S. D. Burton, and J. Harte (2012), Persistence of soil organic matter in eroding versus depositional landform positions, *J. Geophys. Res.*, *117*, G02019, doi:10.1029/2011JG001790.

Bettis, E. A., D. R. Muhs, H. M. Roberts, and A. G. Wintle (2003), Last glacial loess in the conterminous USA, *Quat. Sci. Rev.*, *22*(18), 1907–1946.

Beyer, L., R. Frund, U. Schleuss, and C. Wachendorf (1993), Colluvisols under cultivation in Schleswig-Holstein. 2. Carbon distribution and soil organic matter composition, *J. Plant Nutr. Soil Sci.*, *156*, 213–217.

Billings, S. A., R. W. Buddemeier, D. Richter, K. Van Oost, and G. Bohling (2010), A simple method for estimating the influence of eroding soil profiles on atmospheric CO_2, *Global Biogeochem. Cycles*, *24*, GB2001, doi:10.1029/2009GB003560.

Blaschke, T., and G. J. Hay (2001), Object-oriented image analysis and scale-space: Theory and methods for modeling and evaluating multiscale landscape structure, *Int. Arch. Photogr. Remote Sens.*, *34*(4), W5.

Bortolon, E. S. O., J. Mielniczuk, C. G. Tornquist, F. Lopes, and H. Bergamaschi (2011), Validation of the Century model to estimate the impact of agriculture on soil organic carbon in Southern Brazil, *Geoderma*, *167*, 156–166.

Brown, D. J., E. R. Hunt, R. C. Izaurralde, K. H. Paustian, C. W. Rice, B. L. Schumaker, and T. O. West (2010), Soil organic carbon change monitored over large areas, *Eos Trans. AGU*, *91*(47), 441–442, doi:10.1029/2010EO470001.

Burkart, M., D. James, M. Liebman, and C. Herndl (2005), Impacts of integrated crop-livestock systems on nitrogen dynamics and soil erosion in western Iowa watersheds, *J. Geophys. Res.*, *110*, G0100, doi:10.1029/2004JG000008.

Burke, I. C., C. M. Yonker, W. J. Parton, C. V. Cole, D. S. Schimel, and K. Flach (1989), Texture, climate, and cultivation effects on soil organic matter content in US grassland soils, *Soil Sci. Soc. Am. J.*, *53*(3), 800–805.

Burras, C. L., J. M. McLaughlin, S. A. Wills, M. Barker, and E. C. Brummer (2005), Soil carbon and quality in Seymour and Clarinda soil map units, Chariton Valley, Iowa Final Rep., Chariton Valley RC&D (ISU Project 400-41-71-4216).

Cambardella, C. A., T. B. Moorman, S. S. Andrews, and D. L. Karlen (2004), Watershed-scale assessment of soil quality in the loess hills of southwest Iowa, *Soil Tillage Res.*, *78*(2), 237–247.

Campbell, C. A., B. G. McConkey, R. Zentner, F. Selles, and D. Curtin (1996), Long-term effects of tillage and crop rotations on soil organic C and total N in a clay soil in southwestern Saskatchewan, *Can. J. Soil Sci.*, *76*(1996), 395–401.

Cao, Z. X., Z. J. Li, G. Pender, and P. Hu (2012), Non-capacity or capacity model for fluvial sediment transport, *Water Manage.*, *165*, 193–211.

Celik, I., M. M. Turgut, and N. Acir (2012), Crop rotation and tillage effects on selected soil physical properties of a Typic Haploxerert in an irrigated semi-arid Mediterranean region, *Int. J. Plant Prod.*, *6*(4), 457–480.

Chapin, F. S., III, P. A. Matson, and H. Mooney (2002), *Principles of Terrestrial Ecosystem Ecology*, Springer, New York.

Collins, S., and L. Wallace (1990), *Fire in North American Tallgrass Prairies*, 175 pp., Univ. of Oklahoma Press.

Dalzell, B., T. Filley, and J. Harbor (2007), The role of hydrology in annual organic carbon loads and terrestrial organic matter export from a Midwestern agricultural watershed, *Geochim. Cosmochim. Acta*, *71*(6), 1448–1462, doi:10.1016/j.gca.2006.12.009.

DeLucia, E. H., S. A. Heckathorn, and T. A. Day (1992), Effects of soil temperature on growth, biomass allocation and resource acquisition of *Andropogon gerardii* Vitman, *New Phytol.*, *120*(4), 543–549.

Dermisis, D., O. Abaci, A. N. Papanicolaou, and C. G. Wilson (2010), Evaluating grassed waterway efficiency in southeastern Iowa using WEPP, *Soil Use Manage.*, *26*, 183–192.

Di Stefano, C., and V. Ferro (2002), SW-soil and water: Linking clay enrichment and sediment delivery processes, *Biosyst. Eng.*, *81*(4), 465–479.

Dlugoß, V., P. Fiener, and K. Schneider (2010), Layer-specific analysis and spatial prediction of soil organic carbon using terrain attributes and erosion modeling, *Soc. Am. J.*, *74*, 922–935.

Dlugoß, V., P. Fiener, K. Van Oost, and K. Schneider (2012), Model based analysis of lateral and vertical soil carbon fluxes induced by soil redistribution processes in a small agricultural catchment, *Earth Surf. Processes Landforms*, *37*(2), 193–208.

Du, P., and D. E. Walling (2011), Using 137 Cs measurements to investigate the influence of erosion and soil redistribution on soil properties, *Appl. Radiat. Isot.*, *69*(5), 717–726.

Elhakeem, M., and A. N. Papanicolaou (2009), Estimation of the runoff curve number via direct rainfall simulator measurements in the state of Iowa, USA, *Water Resour. Manage.*, *23*(12), 2455–2473.

Finkner, S. C., M. A. Nearing, G. R. Foster, and J. E. Gilley (1989), A simplified equation for modeling sediment transport capacity, *Trans. ASAE*, *32*(5), 1545–1550.

Flanagan, D. C., and M. A. Nearing (2000), Sediment particle sorting on hillslope profiles in the WEPP model, *Trans. ASAE*, *43*(3), 573–583.

Flanagan, D. C., J. E. Gilley, and T. G. Franti (2007), Water Erosion Prediction Project (WEPP): Development history, model capabilities and future enhancements, *Trans. ASABE*, *50*(5), 1603–1612.

Flanagan, D. C., J. R. Frankenberger, and J. C. Ascough II (2012), WEPP: Model use, calibration and validation, *Trans. ASABE*, *55*, 1463–1477.

Foster, G. R. (1982), Modeling the erosion process, in *Hydrologic Modeling of Small Watersheds*, *Monogr.*, vol. 5, edited by C. T. Haan et al., pp. 297–380, Am. Soc. Agricultural Engineers, St. Joseph, Mich.

Foster, G. R., and L. D. Meyer (1972), Transport of soil particles by shallow flow, *Trans. ASAE*, *15*(1), 99–102.

Foster, G. R., R. A. Young, and W. H. Neibling (1985), Sediment composition for nonpoint source pollution analyses, *Trans. ASAE*, *28*(1), 133–139.

Foster, G. R., D. C. Flanagan, M. A. Nearing, L. J. Lane, L. M. Risse, and S. C. Finkner (1995), Hillslope erosion component, in *USDA-Water Erosion Prediction Project: Hillslope Profile and Watershed Model Documentation*, pp. 11.1–11.2, Natl. Soil Erosion Res. Lab., West Lafayette, Ind.

Fox, J. F., and A. N. Papanicolaou (2007), The use of carbon and nitrogen isotopes to study watershed erosion processes, *J. Am. Water Resour. Ascoc.*, *43*(4), 1047–1064.

Fox, J. F., and A. N. Papanicolaou (2008), Application of the spatial distribution of nitrogen stable isotopes for sediment tracing at the watershed scale, *J. Hydrol.*, *358*, 46–55.
Gabet, E. J., and T. Dunne (2003), Sediment detachment by rain power, *Water Resour. Res.*, *39*(1), 1002, doi:10.1029/2001WR000656.
Gete, Z., T. Winter, and D. Flanagan (1999), BPCDG: Breakpoint climate data generator for WEPP using observed standard weather data sets.
Gilley, J. E., D. A. Woolheiser, and D. McWhorter (1985), Interril soil erosion. Part I. Development of model equations, *Trans. ASAE*, *28*, 147–153.
Gregorich, E. G., K. J. Greer, D. W. Anderson, and B. C. Liang (1998), Carbon distribution and losses: Erosion and deposition effects, *Soil Tillage Res.*, *47*, 291–302.
Hancock, G. R., D. Murphy, and K. G. Evans (2010), Hillslope and catchment scale soil organic carbon concentration: An assessment of the role of geomorphology and soil erosion in an undisturbed environment, *Geoderma*, *155*, 36–45.
Handler, A. (1990), USA corn yields, the El Niño and agricultural drought: 1867–1988, *Int. J. Climatol.*, *10*, 819–828, doi:10.1002/joc.3370100804.
Harden, J. W., J. M. Sharpe, and W. J. Parton (1999), Dynamic replacement and loss of soil carbon on eroding cropland, *Global Biogeochem. Cycles*, *13*, 885–901, doi:10.1029/1999GB900061.
Hart, R. H. (2001), Plant biodiversity on shortgrass steppe after 55 years of zero, light, moderate, or heavy cattle grazing, *Plant Ecol.*, *155*(1), 111–118.
Hatfield, J. L., and T. B. Parkin (2012), Spatial variation of carbon dioxide fluxes in corn and soybean fields, *Agric. Sci.*, *3*(8), 986–995.
Heinitz, A. J. (1986), Floods in south-central Iowa, *U.S. Geol. Surv. Open File Rep. 85–100*, 95 p.
Highland, J. D., and R. I. Dideriksen (1967), *Soil Survey of Iowa County, Iowa*, U.S. Department of Agriculture, Soil Conservation Service, in cooperation with the Iowa Agricultural Experiment Station, Washington, D. C.
Holland, E. A., and D. C. Coleman (1987), Litter placement effects on microbial and organic matter dynamics in an agroecosystem, *Ecology*, *68*, 425–433.
Houghton, R. A. (2008), Carbon flux to the atmosphere from land-use changes, in *TRENDS: A Compendium of Data on Global Change*, Carbon Dioxide Information Analysis Center, Oak Ridge Natl. Lab., U.S. Dep. of Energy, Oak Ridge, Tenn.
Hu, Y., W. Fister, and N. J. Kuhn (2013), Temporal variation of SOC enrichment from interrill erosion over prolonged rainfall simulations, *Agriculture*, *3*, 726–740.
Huang, C., C. Gascuel-Odoux, and S. Cros-Cayot (2002), Hillslope topographic and hydrologic effects on overland flow and erosion, *Catena*, *46*(2), 177–188.
Huehn, M. (1993), Harvest index versus grain straw-ratio. Theoretical comments and experimental results on the comparison of variation, *Euphytica*, *68*, 27–32.
Iowa Environmental Mesonet (IEM) (2015), Climodat reports. [Available at http://mesonet.agron.iastate.edu/climodat/ Accessed: 2015.]
Jacinthe, P. A., R. Lal, and L. B. Owens (2009), Application of stable isotope analysis to quantify the retention of eroded carbon in grass filters at the North Appalachian experimental watersheds, *Geoderma*, *148*, 405–441.
Jacinthe, P., and R. Lal (2001), A mass balance approach to assess carbon dioxide evolution during erosional events, *Land Degrad Dev.*, *12*, 329–339.
Jarecki, M. K., T. B. Parkin, A. S. K. Chan, J. L. Hatfield, and R. Jones (2008), Greenhouse gas emissions from two soils receiving nitrogen fertilizer and swine manure slurry, *J. Environ. Qual.*, *37*, 1432–1438.
Kaiser, J. (2011), Big bluestem and indiangrass for biomass production by variety selection and establishment methods for Missouri, Illinois, and Iowa Agronomy Tech. Note 39.
Karlen, D. L., J. L. Kovar, C. A. Cambardella, and T. S. Colvin (2013), Thirty-year tillage effects on crop yield and soil fertility indicators, *Soil Tillage Res.*, *130*, 24–41.
Keeney, D. R., and J. L. Hatfield (2008), The nitrogen cycle historical perspective and current and potential future concerns, in *Nitrogen in the Environment: Sources Problems and Management*, pp. 1–18, Academic Press Elsevier Inc., Amsterdam, Netherlands.
Kidwell, M. R., M. A. Weltz, and D. P. Guertin (1997), Estimation of Green-Ampt effective hydraulic conductivity for rangelands, *J. Range Manage*, *50*, 290–299.
Kravchenko, A. N., and G. P. Robertson (2011), Whole-profile soil carbon stocks: The danger of assuming too much from analyses of too little, *Soil Sci. Soc. Am. J.*, *75*, 235–240.
Kuhn, N. J., T. Hoffmann, W. Schwanghart, and M. Dotterweich (2009), Agricultural soil erosion and global carbon cycle: Controversy over?, *Earth Surf. Processes Landforms*, *34*(7), 1033–1038.
Lal, R. (1995), Tillage systems in the tropics, in *Land and Water Development*, vol. 71, pp. 206, FAO Soils Bull., Rome, Italy.
Lal, R. (2004), Soil carbon sequestration impacts on global climate change and food security, *Science*, *304*(5677), 1623–1627.
Lal, R. (2005), Soil erosion and carbon dynamics, *Soil Tillage Res.*, *81*(2), 137–142, doi:10.1016/j.still.2004.09.002.
Lal, R. (2006), Influence of soil erosion on carbon dynamics in the world, in *Advances in Soil Science: Soil Erosion and Carbon Dynamics*, edited by E. J. Roose et al., pp. 23–36, Taylor and Francis, Boca Raton, Fla.
Lal, R. (2011), Agronomic interactions with CO_2 sequestration, in *Encyclopedia of Sustainability Science and Technology*, edited by R. A. Meyers, pp. 31–37, Springer, Berlin, Germany.
Latshaw, W., and E. Miller (1924), Elemental composition of the corn plant, *J. Agric. Res*, *XXVII*, 845–860.
Lauer, J. (2002), Methods for calculating corn yield, agronomy advice, Univ. Of Wisconsin-Madison. [Available at http://corn.agronomy.wisc.edu/AA/pdfs/A033.pdf, Accessed May 2015.]
Li, C., S. Frolking, G. J. Crocker, P. R. Grace, J. Klír, M. Körchens, and P. R. Poulton (1997), Simulating trends in soil organic carbon in long-term experiments using the DNDC model, *Geoderma*, *81*(1), 45–60.
Li, J., S. Ziegler, C. S. Lane, and S. A. Billings (2012), Warming-enhanced preferential microbial mineralization of humified boreal forest soil organic matter: Interpretation of soil profiles along a climate transect using laboratory incubations, *J. Geophys. Res.*, *117*, G02008, doi:10.1029/2011JG001769.
Lindley, M. R., B. J. Barfield, and B. N. Wilson (1995), Surface impoundment element model description, in *USDA-Water Erosion Prediction Project: Hillslope Profile and Watershed Model Documentation, Rep*, vol. 10, edited by D. C. Flanagan and M. A. Nearing, chap. 14, pp. 1–28, Natl. Soil Erosion Res. Lab., Agric. Res. Serv., U.S. Dep. of Agric, West Lafayette, Ind.
Liu, S., N. Bliss, E. Sundquist, and T. G. Huntington (2003), Modeling carbon dynamics in vegetation and soil under the impact of soil erosion and deposition, *Global Biogeochem. Cycles*, *17*(2), 1074, doi:10.1029/2002GB002010.
Liu, S., Z. Tan, Z. Li, S. Zhao, and W. Yuan (2011), Are soils of Iowa USA currently a carbon sink or source? Simulated changes in SOC stock from 1972 to 2007, *Agric. Ecosyst. Environ.*, *140*, 106–112, doi:10.1016/j.agee.2010.11.017.
Logsdon, S. D., and D. L. Karlen (2004), Bulk density as a soil quality indicator during conversion to no-tillage, *Soil Tillage Res.*, *78*(2), 143–149.

Macha, D., and L. Cihacek (2009), Carbon storage in plant and soil components of selected grass monocultures SSSA AnMtgsAbsts 2009.53321, ASA, CSSA, and SSSA, Madison, Wis.
Machinet, G. E., I. Bertrand, B. Chabbert, and S. Recous (2009), Decomposition in soil and chemical changes of maize roots with genetic variations affecting cell wall quality, *Eur. J. Soil Sci.*, *60*, 176–185.
Mangan, J. M., J. T. Overpeck, R. S. Webb, C. Wessman, and A. F. Goetz (2004), Response of Nebraska sand hills natural vegetation to drought, fire, grazing, and plant functional type shifts as simulated by the century model, *Clim. Change*, *63*(1–2), 49–90.
Manies, K. L., J. W. Harden, L. Kramer, and W. J. Parton (2001), Carbon dynamics within agricultural and native sites in the loess region of western Iowa, *Global Change Biol.*, *7*, 545–555.
Mann, L. K. (1986), Changes in soil carbon after cultivation, *Soil Sci.*, *142*, 279–288.
Markstrom, S. L., et al. (2012), Integrated watershed-scale response to climate change for selected basins across the United States, *U.S. Geol. Surv. Sci. Invest. Rep.* 2011–5077, 143 pp.
Martinotti, W., M. Camusso, L. Guzzi, L. Patrolecco, and M. Pettine (1997), C, N and their stable isotopes in suspended and sedimented matter from the Poestuary [Italy], *Water Air Soil Pollut.*, *99*, 325–332.
Melillo, J. M., J. D. Aber, and J. F. Muratore (1982), Nitrogen and lignin control of hardwood leaf litter decomposition dynamics, *Ecology*, *63*, 621–626.
Metherell, A. K., L. A. Harding, C. V. Cole, and W. J. Parton (1993), CENTURY soil organic matter model environment, technical documentation, agroecosystem version 4.0 Great Plains System Research Unit, Tech. Rep. No. 4. USDA-ARS, Fort Collins, Colo., p. 250.
Metting, B., J. Smith, and J. Amthor (1999), Science needs and new technology of soil carbon sequestration, in *Carbon Sequestration in Soils: Science, Monitoring, and Beyond*, *Proc. St. Michaels Workshop, December 1998*, edited by N. Rosenberg et al., Coordinated by Pacific Northwest Natl. Lab., Oak Ridge Natl. Lab., and the Council for Agric. Sci. Technol., Batelle Press, Columbus, Ohio.
Monreal, C. M., R. P. Zentner, and J. A. Robertson (1997), An analysis of soil organic matter dynamics in relation to management, erosion and yield of wheat in long-term crop rotation plots, *Can. J. Soil Sci.*, *77*(4), 553–63.
Moore, I. D., and G. J. Burch (1986), Sediment transport capacity of sheet and rill flow: Application of unit stream power theory, *Water Resour. Res.*, *22*, 1350–1360, doi:10.1029/WR022i008p01350.
Mutel, C. F. (2010), *A Watershed Year: Anatomy of the Iowa Floods of 2008*, Univ. of Iowa Press, Iowa City, Iowa.
Nadeu, E., J. de Vente, M. Martínez-Mena, and C. Boix-Fayos (2011), Exploring particle size distribution and organic carbon pools mobilized by different erosion processes at the catchment scale, *J. Soils Sediments*, *11*(4), 667–678, doi:10.1007/s11368-011-0348-1.
National Agricultural Statistics Service (NASS) (2012), National Agricultural Statistics Service. [Available at http://www.nass.usda.gov/, Accessed December, 2012.]
Navas, A., L. Gaspar, L. Quijano, M. López-Vicente, and J. Machín (2012), Patterns of soil organic carbon and nitrogen in relation to soil movement under different land uses in mountain fields (South Central Pyrenees), *Catena*, *94*, 43–52.
Nearing, M. A., and A. D. Nicks (1998), Evaluation of the Water Erosion Prediction Project (WEPP) model for hillslopes, in *Modelling Soil Erosion*, *NATO ASI Ser., Ser. I*, vol. 55, edited by W. J. Boardman and D. T. Favis-Mortlock, pp. 45–56, Springer, Berlin.
Neitsch, S. L., J. G. Arnold, J. R. Kiniry, J. R. Williams, and K. W. King (2002), Soil and Water Assessment Tool theoretical documentation TWRI Report TR-191. Texas Water Resour. Inst., College Station, Tex.
Olchin, G., S. Ogle, S. Frey, T. Filley, K. Paustian, and J. Six (2008), Residue carbon stabilization in soil aggregates of no-till and tillage management of dryland cropping systems, *Soil Sci. Soc. Am. J.*, *72*, 507–513.
O'neal, B. (2009), Quaternary stratigraphy and pedology of Clear Creek in Iowa County Iowa Graduate Thesis Dissertations, Pap. 10937.
Osunbitan, J. A., D. J. Oyedele, and K. O. Adekalu (2005), Tillage effects on bulk density, hydraulic conductivity and strength of a loamy sand soil in southwestern Nigeria, *Soil Tillage Res.*, *82*(1), 57–64.
Owens, L. B., R. W. Malone, D. L. Hothem, G. C. Starr, and R. Lal (2002), Sediment carbon concentration and transport from small watersheds under various conservation tillage practices, *Soil Tillage Res*, *67*(1), 65–73.
Palis, R. G., G. Okwach, C. W. Rose, and P. G. Saffigna (1990), Soil erosion processes and nutrient loss. 1. The interpretation of enrichment ratio and nitrogen loss in runoff sediment, *Aust. J. Soil Res.*, *28*(4), 623–639.
Palis, R. G., H. Ghandiri, C. W. Rose, and P. G. Saffigna (1997), Soil erosion and nutrient loss. III. Changes in the total enrichment ratio of total nitrogen and organic carbon under rainfall detachment and entrainment, *Aust. J. Soil Res.*, *35*, 891–905.
Pansu, M., J. Gautheyrou, and J. Y. Loyer (2001), *Soil Analysis*, Balkema, Netherlands.
Papanicolaou, A. N., and O. Abaci (2008), Upland erosion modeling in a semi-humidenvironment via the Water Erosion Prediction Project, *J. Irrig. Drain. Eng.*, *134*(6), 796–806, doi:10.1061/(ASCE)0733-9437(2008)134:6(796.
Papanicolaou, A. N., A. Bdour, and E. Wicklein (2004), One-dimensional hydrodynamic/sediment transport model applicable to steep mountain streams, *J. Hydraul. Res.*, *42*(4), 357–375.
Papanicolaou, A. N., M. Elhakeem, C. G. Wilson, C. L. Burras, and B. Oneal (2008), Observations of soils at the hillslope scale in the Clear Creek watershed in Iowa, USA, *Soil Surv. Horizons*, *49*, 83–86.
Papanicolaou, A. N., C. G. Wilson, O. Abaci, M. Elhakeem, and M. Skopec (2009), Soil quality in Clear Creek, IA: SOM loss and soil quality in the Clear Creek, IA Experimental Watershed, *J. Iowa Acad. Sci.*, *116*(1–4), 14–26.
Papanicolaou, A. N., J. T. Sanford, D. C. Dermisis, and G. A. Mancilla (2010), A 1-D morphodynamic model for rill erosion, *Water Resour. Res.*, *46* W09541, doi:10.1029/2009WR008486.
Papanicolaou, A. T. N., M. Elhakeem, C. G. Wilson, C. L. Burras, L. T. West, H. H. Lin, and B. E. Oneal (2015), Spatial variability of saturated hydraulic conductivity at the hillslope scale: Understanding the role of land management and erosional effect, *Geoderma*, *243*, 58–68.
Parkin, T. B. (1993), Spatial variability of microbial processes in soil—A review, *J. Environ. Qual.*, *22*(3), 409–417.
Parton, W. J., D. S. Schimel, C. V. Cole, and D. S. Ojima (1987), Analysis of factors controlling soil organic matter levels in great plains grasslands, *Soil Sci. Soc. Am. J.*, *51*, 1173–1179.
Parton, W., W. L. Silver, I. C. Burke, L. Grassens, M. E. Harmon, and W. S. Currie (2007), Global-scale similarities in nitrogen release patterns during long-term decomposition, *Science*, *315*, 361–364.
Paustian, K., W. J. Parton, and J. Persson (1992), Modeling soil organic matter in organic-amended and nitrogen-fertilized long-term plots, *Soil Sci. Soc. Am. J.*, *56*, 476–488.
Paustian, K., N. H. Ravindranath, and A. van Amstel (2006), Agriculture, forestry and other land use [AFOLU], in *2006 IPCC Guidelines for National Greenhouse Gas Inventories*, vol. 4, edited by S. Eggleston et al., Inst. for Global Environ. Strategies, Hayama, Japan.
Pieri, L., M. Bittelli, J. Q. Wu, S. Dun, D. C. Flanagan, P. R. Pisa, and F. Salvatorelli (2007), Using the Water Erosion Prediction Project (WEPP) model to simulate field-observed runoff and erosion in the Apennines mountain range, Italy, *J. Hydrol.*, *336*(1), 84–97.
Polyakov, V., and R. Lal (2004), Modeling soil organic matter dynamics as affected by soil water erosion, *Environ. Int.*, *30*(4), 547–556.

Prince, S. D., J. Haskett, M. Steininger, H. Strand, and R. Wright (2001), Net primary production of U.S. Midwest croplands from agricultural harvest data, *Ecol. Appl.*, *11*, 1194–1205.
Quine, T. A., D. E. Walling, and X. Zhang (1999), Tillage erosion, water erosion and soil quality on cultivated terraces near Xifeng in the Loess Plateau, China, *Land Degrad. Dev.*, *10*(3), 251–274.
Reichstein, M., M. Bahn, P. Ciais, D. Frank, M. D. Mahecha, S. I. Seneviratne, and M. Wattenbach (2013), Climate extremes and the carbon cycle, *Nature*, *500*(7462), 287–295.
Reicosky, D. C., W. D. Kemper, G. W. Langdale, C. L. Douglas Jr., and P. E. Rasmussen (1995), Soil organic matter changes resulting from tillage and biomass production, *J. Soil Water Conserv.*, *50*(1), 253–261.
Rhoton, F. E., M. J. Shipitalo, and D. L. Lindbo (2002), Runoff and soil loss from midwestern and southeastern US silt loam soils as affected by tillage practice and soil organic matter content, *Soil Tillage Res.*, *66*, 1–11.
Richter, D. D., D. Markewitz, S. E. Trumbore, and C. G. Wells (1999), Rapid accumulation and turnover of soil carbon in a re-establishing forest, *Nature*, *400*, 56–58, doi:10.1038/21867.
Rieke-Zapp, D. H., and M. A. Nearing (2005), Slope shape effects on erosion, *Soil Sci. Soc. Am. J.*, *69*(5), 1463–1471.
Römkens, M. J. M., K. Helming, and S. N. Prasad (2002), Soil erosion under different rainfall intensities, surface roughness, and soil water regimes, *Catena*, *46*(2–3), 103–123, doi:10.1016/s0341-8162(01)00161-8.
Rosenzweig, C., F. N. Tubiello, R. Goldberg, E. Mills, and J. Bloomfield (2002), Increased crop damage in the US from excess precipitation under climate change, *Global Environ. Change*, *12*(3), 197–202.
Rupnow, J., and C. W. Knox (1975), *The Growing of America: 200 Years of U.S. Agriculture*, Johnson Hill Press, Fort Atkinson, Wis distributed by Nasco.
Salinas-García, J. R., J. J. Velázquez-García, M. Gallardo-Valdez, P. Díaz-Mederos, F. Caballero-Hernández, L. M. Tapia-Vargas, and E. Rosales-Robles (2002), Tillage effects on microbial biomass and nutrient distribution in soils under rain-fed corn production in central western Mexico, *Soil Tillage Res.*, *66*, 143–152.
Santhi, C., J. G. Arnold, J. R. Williams, W. A. Dugas, R. Srinivasan, and L. M. Hauck (2001), Validation of the SWAT model on a large river basin with point and nonpoint sources, *J. Am. Water Resour. Assoc.*, *37*(5), 1169–1188.
Saxena, D., and G. Stotzky (2001), Bt corn has a higher lignin content than non-Bt corn, *Am. J. Botany*, *88*(9), 1704–1706.
Schiettecatte, W., D. Gabriels, W. M. Cornelis, and G. Hofman (2008), Enrichment of organic carbon in sediment transport by interrill and rill erosion processes, *Soil Sci. Soc. Am. J.*, *72*, 50–55.
Schlesinger, W. H. (1990), Evidence from chronosequence studies for a low carbon-storage potential of soils, *Nature*, *348*(6298), 232–234.
Schurgers, G., A. Arneth, and T. Hickler (2011), Effect of climate-driven changes in species composition on regional emission capacities of biogenic compounds, *J. Geophys. Res.*, *116*, D22304, doi:10.1029/2011JD016278.
Schwärzel, K., S. Carrick, A. Wahren, K. H. Feger, G. Bodner, and G. Buchan (2011), Soil hydraulic properties of recently tilled soil under cropping rotation compared with two-year pasture, *Vadose Zone J.*, *10*(1), 354–366.
Six, J., R. Conant, E. Paul, and K. Paustian (2002), Stabilization mechanisms of soil organic matter: Implications for C-saturation of soils, *Plant Soil*, *241*, 155–176.
Smith, J. L., and E. A. Paul (1990), The significance of soil microbial biomass estimations, in *Soil Biochemistry*, vol. 6, edited by J. M. Bollag and G. Stotzky, pp. 357–396, Marcel Dekker Inc., New York.
Smith, S. V., W. H. Renwick, R. W. Buddemeier, and C. J. Crossland (2001), Budgets of soil erosion and deposition for sediments and sedimentary organic carbon across the conterminous United States, *Global Biogeochem. Cycles*, *15*, 697–707, doi:10.1029/2000GB001341.
Sorensen, L. H. (1981), Carbon-nitrogen relationships during the humification of cellulose in soils containing different amounts of clay, *Soil Biol. Biochem.*, *13*(4), 313–321.
Sperow, M., M. Eve, and K. Paustian (2003), Potential soil C sequestration on US agricultural soils, *Clim. Change*, *57*(3), 319–339.
Sposito, G. (1989), *The Chemistry of Soils*, 277 pp., Oxford Univ. Press, New York.
Stavi, I., and R. Lal (2011), Variability of soil physical quality in uneroded, eroded, and depositional cropland sites, *Geomorphology*, *125*(1), 85–91.
Stewart, C. E., K. Paustian, R. T. Conant, A. F. Plante, and J. Six (2007), Soil carbon saturation: Concept, evidence and evaluation, *Biogeochemistry*, *86*, 19–31.
Stinner, B. R., G. D. Hoyt, and R. L. Todd (1983), Changes in some chemical properties following a 12-year fallow: A 2-year comparison of conventional tillage and no-tillage agroecosystems, *Soil Tillage Res.*, *3*, 277–290.
Teixeira, P. C., and R. K. Misra (1997), Erosion and sediment characteristics of cultivated forest soils as affected by the mechanical stability of aggregates, *Catena*, *30*, 119–134.
Thevenot, M., M. F. Dignac, and C. Rumpel (2010), Fate of lignins in soils: A review, *Soil Biol. Biochem.*, *42*(8), 1200–1211.
Thompson, S., G. Katul, and S. M. McMahon (2008), Role of biomass spread in vegetation pattern formation within arid ecosystems, *Water Resour. Res.*, *44*, W10421, doi:10.1029/2008WR006916.
Thompson, S., G. Katul, and A. Porporato (2010), Role of microtopography in rainfall-runoff partitioning: An analysis using idealized geometry, *Water Resour. Res.*, *46*, W07520, doi:10.1029/2009WR008835.
Tivy, J. (1990), *Agricultural Ecology*, 288 pp., Longman Sci. Tech., London.
Tornquist, C. G., J. Mielniczuk, and C. E. P. Cerri (2009), Modeling soil organic carbon dynamics in Oxisols of Ibirubá (Brazil) with the Century model, *Soil Tillage Res.*, *105*, 33–43.
Trautmann, N. M., K. S. Porter, and R. J. Wagenet (1985), *Modern Agriculture: Its Effects on the Environment*, Cornell Univ. Cooperative Extension, Ithaca, New York.
Vaccari, F. P., E. Lugato, B. Gioli, L. D'Acqui, L. Genesio, P. Toscano, and F. Miglietta (2012), Land use change and soil organic carbon dynamics in Mediterranean agro-ecosystems: The case study of Pianosa Island, *Geoderma*, *175*, 29–36.
van Groenigen, K. J., A. Hastings, D. Forristal, B. Roth, M. Jones, and P. Smith (2011), Soil C storage as affected by tillage and straw management: An assessment using field measurements and model predictions, *Agric. Ecosyst. Environ.*, *140*, 218–222.
Van Oost, K., G. Govers, and P. Desmet (2000), Evaluating the effects of landscape structure on soil erosion by water and tillage, *Landscape Ecol.*, *15*(6), 579–591.
Van Oost, K., G. Govers, T. A. Quine, G. Heckrath, J. Olesen, and R. Merckx (2005), Landscape-scale modeling of carbon cycling under the impact of soil redistribution: The role of tillage erosion, *Global Biogeochem. Cycles*, *19*, GB4014, doi:10.1029/2005GB002471.
Van Oost, K., O. Cerdan, and T. A. Quine (2009), Accelerated sediment fluxes by water and tillage erosion on European agricultural land, *Earth Surf. Processes Landforms*, *34*(12), 1625–1634.
Van Oost, K. V., G. Govers, T. A. Quine, and G. Heckrath (2006), Modeling soil erosion induced carbon fluxes between soil and atmosphere on agricultural land using SPEROS-C, in *Soil Erosion and Carbon Dynamics*, edited by E. J. Roose et al., pp. 37–51, CRC Press, Boca Raton, Fla.

Van Veen, J. A., J. N. Ladd, and M. J. Frissel (1984), Modelling C and N turnover through the microbial biomass in soil, *Plant Soil*, *76*(1–3), 257–274.
Vázquez, E. V., J. V. Miranda, and A. P. Gónzalez (2005), Characterizing anisotropy and heterogeneity of soil surface microtopography using fractal models, *Ecol. Model.*, *182*(3), 337–353.
Wäldchen, J., I. Schöning, M. Mund, M. Schrumpf, S. Bock, N. Herold, and E. D. Schulze (2012), Estimation of clay content from easily measurable water content of air-dried soil, *J. Plant Nutr. Soil Sci.*, *175*(3), 367–376.
Wang, Z., G. Govers, K. V. Oost, W. Clymans, A. V. Putte, and R. Merckx (2013), Soil organic carbon mobilization by interrill erosion: Insights from size fractions, *J. Geophys. Res. Earth Surf.*, *118*, 348–360, doi:10.1029/2012JF002430.
Wang, Z., S. Doetterl, M. Vanclooster, B. van Wesemael, and K. Van Oost (2015), Constraining a coupled erosion and soil organic carbon model using hillslope-scale patterns of carbon stocks and pool composition, *J. Geophys. Res. Biogeosci.*, *120*, 452–465, doi:10.1002/2014JG002768.
Weaver, J. E. (1968), *Prairie Plants and Their Environment*, Univ. of Nebraska Press, Lincoln, Nebr.
Williams, J. R., C. A. Jones, and P. Dyke (1984), Modeling approach to determining the relationship between erosion and soil productivity, *Trans. ASAE*, *27*(1), 129–144.
Wilson, C. G., A. N. T. Papanicolaou, and O. Abaci (2009), SOM dynamics and erosion in an agricultural test field of the Clear Creek, IA watershed, *Hydrol. Earth Syst. Sci. Discuss.*, *6*, 1581–1619.
Xiao, X. M., D. Hollinger, J. Aber, M. Goltz, E. A. Davidson, and Q. Y. Zhang (2004), Satellite-based modeling of gross primary production in an evergreen needleleaf forest, *Remote Sens. Environ.*, *89*(4), 519–534.
Yadav, V., and G. P. Malanson (2009), Modeling impacts of erosion and deposition on soil organic carbon in the Big Creek Basin of southern Illinois, *Geomorphology*, *106*(3), 304–314.
Yalin, M. S. (1963), An expression for bed-load transportation, *J. Hydr. Eng. Div-ASCE*, *89*, 221–250.
Yalin, M. S. (1977), *Mechanics of Sediment Transport*, 2nd ed., 298 pp., Pergamon Press, New York.
Yang, C. T. (1973), Incipient motion and sediment transport, *J. Hydrol. Eng. Div-ASCE*, *99*(10), 1679–1704.
Yoo, K., R. Amundson, A. M. Heimsath, and W. E. Dietrich (2005), Erosion of upland hillslope soil organic carbon: Coupling field measurements with a sediment transport model, *Global Biogeochem. Cycles*, *19*, GB3003, doi:10.1029/2004GB002271.
Young, C. J., J. A. Schumacher, T. E. Schumacher, T. C. Kaspar, G. W. McCarty, S. Liu, and D. Napton (2014), Evaluation of a model framework to estimate soil and soil organic carbon redistribution by water and tillage using 137Cs in two U.S. Midwest agricultural fields, *Geoderma*, *232*, 437–448.
Zhang, G. H., B. Y. Liu, G. B. Liu, X. W. He, and M. A. Nearing (2003), Detachment of undisturbed soil by shallow flow, *Soil Sci. Soc. Am. J.*, *67*, 713–719.
Zhang, H., S. Liu, W. Yuan, W. Dong, A. Ye, X. Xie, Y. Chen, D. Liu, W. Cai, and Y. Mao (2014), Inclusion of soil carbon lateral movement alters terrestrial carbon budget in China, *Sci. Rep.*, *4*, doi:10.1038/srep07247.
Zhang, X., Z. Li, Z. Tang, G. Zeng, J. Huang, W. Guo, and A. Hirsh (2013), Effects of water erosion on the redistribution of soil organic carbon in the hilly red soil region of southern China, *Geomorphology*, *197*, 137–144.
Zheng, Y., X. Luo, W. Zhang, B. Wu, F. Han, Z. Lin, and X. Wang (2012), Enrichment behavior and transport mechanism of soil-bound PAHs during rainfall-runoff events, *Environ. Pollut.*, *171*, 85–92.